



University of Warwick institutional repository: <http://go.warwick.ac.uk/wrap>

This paper is made available online in accordance with publisher policies. Please scroll down to view the document itself. Please refer to the repository record for this item and our policy information available from the repository home page for further information.

To see the final version of this paper please visit the publisher's website. Access to the published version may require a subscription.

Author(s): J. Girven, B. T. Gänsicke, D. Steeghs, D. Koester

Article Title: DA white dwarfs in Sloan Digital Sky Survey Data Release 7 and a search for infrared excess emission

Year of publication: 2011

Link to published article:

<http://dx.doi.org/10.1111/j.1365-2966.2011.19337.x>

Publisher statement: 'The definitive version is available at www.blackwell-synergy.com'.

DA white dwarfs in SDSS DR7 *and* a search for infrared excess emission

J. Girven¹, B. T. Gänsicke¹, D. Steeghs¹, D. Koester²

¹ *Department of Physics, University of Warwick, Coventry CV4 7AL, UK*

² *Institut für Theoretische Physik und Astrophysik, University of Kiel, 24098 Kiel, Germany*

Started 2009

ABSTRACT

We present a method which uses colour-colour cuts on SDSS photometry to select white dwarfs with hydrogen rich (DA) atmospheres without the recourse to spectroscopy. This method results in a sample of DA white dwarfs that is 95% complete at an efficiency of returning a true DA white dwarf of 62%. The approach was applied to SDSS Data Release 7 for objects with and without SDSS spectroscopy. This led to 4636 spectroscopically confirmed DA white dwarfs with $g \leq 19$; a $\sim 70\%$ increase compared to Eisenstein et al.'s 2006 sample. Including the photometric-only objects, we estimate a factor of 3 increase in DA white dwarfs. We find that the SDSS spectroscopic follow-up is 44% complete for DA white dwarfs with $T_{\text{eff}} \gtrsim 8000\text{K}$. We further cross-correlated the SDSS sample with Data Release 8 of the UKIDSS Large Area Survey. The spectral energy distributions of both subsets, with and without SDSS spectroscopy, were fitted with white dwarf models to determine the fraction of DA white dwarfs with low-mass stellar companions or dusty debris discs via the detection of excess near-infrared emission. From the spectroscopic sample we find that 2.0% of white dwarfs have an excess consistent with a brown dwarf type companion, with a firm lower limit of 0.8%. From the white dwarfs with photometry only, we find that 1.8% are candidates for having brown dwarf companions. Similarly, both samples show that $\sim 1\%$ of white dwarfs are candidates for having a dusty debris disc.

Key words: Stars: individual: white dwarfs – infrared excess

1 INTRODUCTION

White dwarfs are the most common stellar remnants in the Galaxy, having descended from main sequence stars with $0.8M_{\odot} \lesssim M \lesssim 8M_{\odot}$. Of these, hydrogen rich (DA) white dwarfs make up the vast majority. Large samples of white dwarfs are particularly useful in many studies, for example constraining the luminosity function, which in turn can be used to determine the ages of many Galactic populations (e.g. Winget et al. 1987; Oswalt et al. 1996; De Gennaro et al. 2008). The low luminosity of white dwarfs also makes them ideal targets for searches of low-mass companions, such as pioneered by Probst & O'Connell (1982). The companion mass distribution is thought to drop near the low-mass end ($\sim 0.1M_{\odot}$), and the fraction of FGK stars with substellar companions estimated from radial velocity surveys is $\lesssim 1\%$ (e.g. Marcy & Butler 2000; Grether & Lineweaver 2006), though Metchev & Hillenbrand (2009) suggest that substellar companions are more frequent at larger orbital separations. Because white dwarfs are the progeny of main-sequence stars with masses of up to $8M_{\odot}$, studies of white dwarf binaries

can probe the companion mass function over a wide range of (initial) host star masses. Currently, only four white dwarfs are confirmed to have (non-interacting) substellar companions (Becklin & Zuckerman 1988; Farihi & Christopher 2004; Maxted et al. 2006; Steele et al. 2009, but see Luhman et al. 2011 for a very low-mass candidate), and the fraction of white dwarfs with brown dwarf companions appears to be consistent with the low number found around FGK stars (Farihi et al. 2005; Hoard et al. 2007).

While white dwarfs are also excellent candidates for searches of Jovian planets (e.g. Ignace 2001; Burleigh et al. 2002), no planet has yet been unambiguously discovered around a white dwarf (Burleigh et al. 2008; Hogan et al. 2009; Mullally et al. 2009). However, ~ 15 white dwarfs are known to exhibit infrared flux excesses that can not be explained by the presence of low-mass (planetary or substellar) companions (Farihi et al. 2009). The first such infrared excess was found around G 29-38 and tentatively associated with a brown dwarf companion (Zuckerman & Becklin 1987). Using the fact that G 29-38 is a pulsating white dwarf, Graham et al. (1990) demonstrated that the obser-

vations are best explained with the presence of circumstellar dust heated by the white dwarf, and proposed the disruption of a large asteroid as the origin of the dust. Koester et al. (1997) detected metals in the photosphere of G 29-38, demonstrating that the white dwarf is accreting circumstellar material. The scenario of the tidal disruption of rocky asteroids has been refined by Jura (2003), and is now the generally accepted interpretation of the growing number of metal-polluted white dwarfs with infrared excess. Farihi et al. (2009) estimate that 1 – 3% of all white dwarfs with cooling ages below 0.5 Gyr should exhibit infrared excess related to the tidal disruption of asteroids. The location of the debris material within the white dwarf tidal disruption radius for a rocky asteroid has ultimately been confirmed by Gänsicke et al. (2006b) who detected Doppler-broadened Ca II emission lines from a gaseous component of the circumstellar disc in SDSSJ122859.93+104032.9, a metal-polluted white dwarf with infrared excess (Brinkworth et al. 2009).

In this paper, we use the Sloan Digital Sky Survey (SDSS) to first identify a method to select hydrogen-rich (DA) white dwarfs using photometric criteria, and then determine those with infrared flux excess in the UKIRT Infrared Deep Sky Survey (UKIDSS). Our method is sensitive to unresolved M and L-type companions and to warm debris discs. The long-term goal of this project is to increase the number of such objects available for detailed follow-up studies, and to provide a more detailed understanding of the frequency of both substellar companions to and planetary debris discs around white dwarfs.

The structure of the paper is as follows: In Sect. 2 we discuss the three surveys that are utilised in this paper; the Sloan Digital Sky Survey, the UKIRT Infrared Deep Sky Survey and the Wide-field Infrared Survey Explorer (WISE). The method for selecting DA white dwarfs from SDSS DR7 is outlined in Sect. 3 along with a discussion of the spectroscopic completeness of SDSS with respect to DA white dwarfs. The procedure for cross-matching objects from SDSS with UKIDSS is demonstrated in Sect. 4. Identifying which white dwarfs show an IR excess and the method for fitting these excesses is given in Sect. 5. Further to this, Sect. 5.4 discusses comparisons between the spectroscopic and photometric fitting methods, including how contaminants were dealt with. A summary of the overall numbers of objects at each stage of the process is given in Sect. 5.5. Some notes on interesting objects discovered in this work are given in Sect. 6. A comparison between the work herein and the white dwarf-main sequence star catalogue of Rebassa-Mansergas et al. (2010) is made in Sect. 7. Objects that are detected in WISE are discussed in Sect. 8. The implications of the DA white dwarf selection and the IR excess selection methods are discussed in Sect. 9. Finally, the conclusions of this work are drawn together in Sect. 10.

2 LARGE AREA SURVEYS

The Sloan Digital Sky Survey (SDSS, York et al. 2000; Stoughton et al. 2002) and the UKIRT Infrared Deep Sky Survey (UKIDSS, Lawrence et al. 2007) are currently the deepest large-area optical and infrared surveys that are publicly available, and we summarise below details of both surveys relevant for our work.

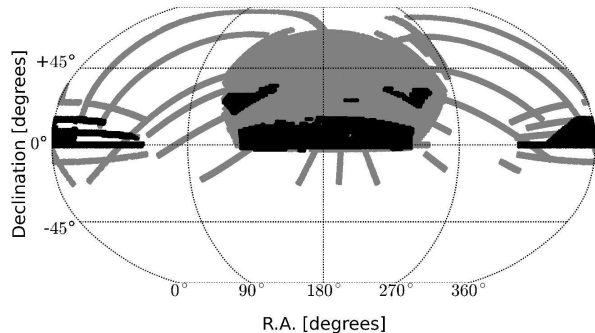


Figure 1. Coverage of the SDSS DR7 (grey) and UKIDSS DR8 LAS (black) in equatorial coordinates.

2.1 SDSS

We have made use of the SDSS Data Release seven (DR7, Abazajian et al. 2009), which represents the final DR of the SDSSII project, including the low-latitude extension SEGUE (Yanny et al. 2009). SDSS DR7 provides *ugriz* photometry for 357 million objects spanning a magnitude range $\sim 15 - 22$ and covering 11500 deg^2 , approximately one-quarter of the celestial sphere, as well as follow-up low-resolution ($R \simeq 1800, 3800 - 9200 \text{ \AA}$) spectroscopy for 1.44 million galaxies, quasars, and stars. We limit our search to point-like sources, and to apparent magnitudes $g \leq 19$, which leaves $\simeq 24$ million unique photometric and 87,000 unique spectroscopic objects. An additional important resource within DR7 are proper motions computed from the USNO-B and SDSS positions.

2.2 UKIDSS

UKIDSS is a set of five near infrared surveys being undertaken with the Wide Field Camera (WFCAM) instrument on the United Kingdom Infrared Telescope (UKIRT) in Hawaii. One of the five sub-surveys, the Large Area Survey (LAS), aims to be the IR counterpart to the SDSS. Here we match SDSS hydrogen-dominated (DA) white dwarfs with UKIDSS LAS as opposed to 2MASS used in similar studies (e.g. Hoard et al. 2007) because a large majority of the SDSS white dwarfs are too faint in the IR for 2MASS to pick up. UKIDSS LAS will eventually provide imaging over 4028 deg^2 in four broad band colours, *Y*, *J*, *H*, and *K*, with limiting (Vega) magnitudes of 20.2, 19.6, 18.8 and 18.2, respectively, which adds a significant increase in depth over 2MASS. Here, we made use of UKIDSS DR8 (see Dye et al. 2006). The overlap between SDSS DR7 and UKIDSS/LAS DR8 is illustrated in Fig. 1, and amounts to ~ 2700 square degrees.

2.3 WISE

The Wide-field Infrared Survey Explorer (WISE) is a NASA Medium-class Explorer mission designed to survey the entire sky in four infrared wavelengths, 3.4, 4.6, 12, and $22 \mu\text{m}$ (Wright et al. 2010). WISE consists of a 40 cm telescope that images all four bands simultaneously every 11 s. It covers nearly every part of the sky a minimum of eight times,

ensuring high source reliability, with more coverage at the ecliptic poles. Astrometric errors are less than 0.5 arcsec with respect to 2MASS (Wright et al. 2010). The preliminary estimated $S/N = 5$ point source sensitivity on the ecliptic is 0.08, 0.1, 0.8, and 5 mJy in the four bands (assuming eight exposures per band; Wright et al. 2010). Sensitivity improves away from the ecliptic due to denser coverage and lower zodiacal background. We took advantage of the preliminary data release (PDR). The SDSS white dwarfs that are the subject of this work are largely too faint to be seen in the 12, and $22\mu\text{m}$ bands and therefore we generally only discuss the 3.4 and $4.6\mu\text{m}$ fluxes.

3 SELECTING DA WHITE DWARFS IN SDSS DR7

The latest catalogue of spectroscopically identified SDSS white dwarfs was based on DR4 (Eisenstein et al. 2006), which comprised roughly half of the sky coverage of DR7. Here, we exploit the much larger footprint of SDSS DR7, and also extend the white dwarf sample to photometric objects without follow-up spectroscopy. We restricted our ambitions to DA white dwarfs for a number of reasons. Firstly, the vast majority of all known white dwarfs belong to the DA class (McCook & Sion 1999). Secondly, determining the atmospheric parameters of DA white dwarfs, T_{eff} and $\log(g)$, from fitting atmosphere models to either spectroscopy (Bergeron et al. 1992) or photometry (Koester et al. 1979) is a well-established and robust procedure. This is essential for the purpose of identifying white dwarfs with infrared excess, as we need to accurately extrapolate the white dwarf flux to the J , H , and K bands. Thirdly, optical spectra of DA white dwarfs are characterised by strong Balmer absorption lines on a blue continuum, and the strong dependence of the Balmer line equivalent widths results in DA white dwarfs occupying a distinct region in colour space.

We have developed a two-pronged approach to identify as many DA white dwarfs with spectroscopy within DR7, and subsequently to select white dwarf candidates which have *ugriz* photometry but were not spectroscopically followed-up by SDSS.

As a start, we retrieved the DR7 spectra and *ugriz* photometry for all white dwarfs with $g \leq 19$ and classified by Eisenstein et al. (2006) as DA or DA_{auto}, corresponding to visually confirmed and automatically classified hydrogen-dominated white dwarfs, respectively. This totals 2889 unique objects, 938 being classified as DA and 1951 DA_{auto}. All spectra were visually inspected to corroborate their DA classification, and we found 99.4% agreement with the classification for white dwarfs by Eisenstein et al. (2006). The 0.6% disagreement primarily comes about from non-DA white dwarfs that were classified as DA_{auto} by Eisenstein et al.’s classification routine. The sample of spectroscopically confirmed DA white dwarfs was then used to trace the locus of DA white dwarfs in the $(u - g, g - r)$, $(g - r, r - i)$, and $(r - i, i - z)$ colour-colour planes. The population of DA white dwarf follows a boomerang-shape in $(u - g, g - r)$ colours, where it is clearly separated from the main sequence, but intersects the quasar population (Fig. 2).

This relatively complex shape was approximated by

the intersection of two 5th-order polynomials (Table 1). In $(g - r, i - r)$ the DA white dwarfs lie along a relatively narrow band, overlapping with the blue end of the main sequence and, to some extent with quasars, which we approximated by the combination of a 2nd and 3rd order polynomial. Finally, in $(r - i, i - z)$, the DA white dwarfs are again located at the blue end of the main sequence, but display a relatively large spread in $i - z$. Visual inspection of the SDSS spectra of the outliers confirms them as DA white dwarfs, though the majority of them are near the faint end of the Eisenstein et al. sample. We decided to include those outliers in our colour-cut, and hence approximated the DA locus by the intersection of three linear relations in $(r - i, i - z)$.

We applied a magnitude cut of $g \leq 19$ as a (conservative) measure, so that each of the SDSS white dwarfs within the UKIDSS footprint would have a significant K -band detection. Finally, we applied a set of recommended data quality flags to the SDSS photometry to minimise contamination by instrumental artifacts and blended stars. Applying the constraint set summarised in Table 1 to DR7 resulted in the selection of 7444 unique spectroscopic objects, which were then visually classified as DA white dwarfs, other (non-DA) white dwarfs, quasars, narrow line hot stars (see below), and other objects (Table 2).

3.1 Narrow Line Hot Stars

The optical spectra of ultra-low mass white dwarfs and very cool DAs, particularly those at low signal-to-noise ratio, can look rather similar to early type main sequence stars, sub-dwarfs, extreme horizontal branch stars or very metal-poor halo stars, which we all lump together as contaminants with the designation “narrow line hot stars” (NLHS). These are particularly dominant at the bright end of the white dwarf banana ($g \leq 16$, see Table 2). While there is noticeable interest in ultra-low mass white dwarfs (e.g. Liebert et al. 2004; Kilic et al. 2007; Marsh et al. 2010), they represent a tiny fraction of all DAs. Given that our aim is to study the bulk population of DA white dwarfs, we make no attempt to accurately classify ultra-low mass white dwarfs. In addition, our colour selection is only complete to effective temperatures above $\sim 8000\text{K}$. Attempting to include much cooler white dwarfs would result in significant contamination from NLHS.

3.2 Overall Completeness and Efficiency

Completeness and efficiency were the key parameters in designing our selection algorithm (Table 1), where we define *completeness* as the fraction of Eisenstein et al.’s DA white dwarfs recovered by our constraints, and *efficiency* as the ratio of spectroscopically confirmed DA white dwarfs to all objects in our colour-magnitude selection. In the case of the spectroscopic DA sample, one may argue that completeness is more important than efficiency because contaminants can be removed through visual spectral classification of all candidate objects. On the other hand, the photometric-only DA sample requires a high level of efficiency to minimise the number of contaminants. We optimised the colour boundaries to maximise both completeness and efficiency, and the constraint set in Table 1 results in a completeness of 95.4%

Table 1. Colour selection for finding DA white dwarfs in *ugriz* space. Objects were selected to be primary objects and point sources. Flags are shown in Hexagesimal notation. These are the standard SDSS “good photometry” flags, as documented on SDSS CASJOBS (Li & Thakar 2008), and were chosen so that the object was detected in BINNED1, and did not have any of the following: EDGE, NOPROFILE, PEAKCENTER, NOTCHECKED, PSF_FLUX_INTERP, SATURATED, or BAD_COUNTS_ERROR.

Colour	constraint	
$(u - g)$	\geq	$-20.653 \times (g - r)^5 + 10.816 \times (g - r)^4 + 15.718 \times (g - r)^3 - 1.294 \times (g - r)^2 - 0.084 \times (g - r) + 0.300$
$(u - g)$	\leq	$-24.384 \times (g - r)^5 - 19.000 \times (g - r)^4 + 3.497 \times (g - r)^3 + 1.193 \times (g - r)^2 + 0.083 \times (g - r) + 0.610$
$(g - r)$	\leq	$-0.693 \times (r - i)^2 + 0.947 \times (r - i) + 0.192$
$(g - r)$	\geq	$-1.320 \times (r - i)^3 + 2.173 \times (r - i)^2 + 2.452 \times (r - i) - 0.070$
$(r - i)$	\geq	-0.560
$(r - i)$	\leq	$0.176 \times (i - z) + 0.127$
$(r - i)$	\leq	$-0.754 \times (i - z) + 0.110$
g	\leq	19
0	\neq	flags & 0x10000000
0	$=$	flags & 0x8100000c00ac

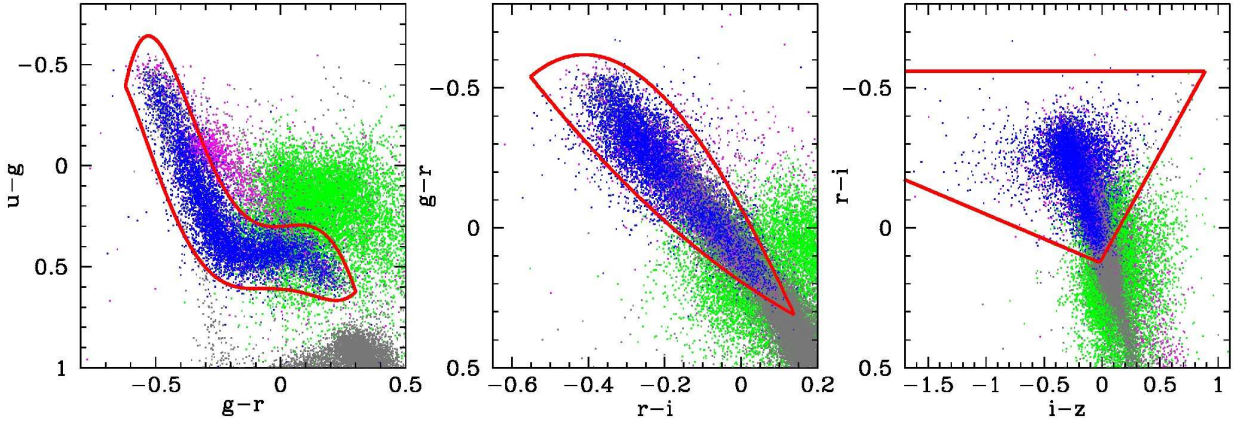


Figure 2. Colour-colour plots illustrating the location of the SDSS spectroscopic objects. DA white dwarfs, non-DA white dwarfs, quasars and main-sequence stars are shown as blue, magenta, green and grey dots respectively. The polynomial colour cuts from Table 1 are overlaid as red lines.

and an efficiency of 62.3% (Table 2). From SDSS DR7, a total 4636 unique spectroscopic DA white dwarfs are contained within the colour-magnitude cuts. This represents a 70% increase in spectroscopic DA white dwarfs with $g \leq 19$ over the Eisenstein et al. (2006) sample. The photometric-only DA white dwarf candidates sample similarly contains 9341 objects. Assuming 62.3% efficiency of the selection, ~ 6000 extra white dwarfs are contained within the sample and therefore the total increase over Eisenstein et al. (2006) is approximately a factor of three. The efficiency is however only a lower limit for the photometric sample because the SDSS is by design almost spectroscopically complete for QSOs, one of our main contaminants. Therefore, QSOs are only a minor contaminant in the photometric-only sample.

The spectral classification and completeness are given as a function of g -magnitude in Table 2. The completeness drops slightly towards larger apparent magnitude because of the larger scatter in the colour-colour diagrams. The fraction of NLHS contaminants is largest at the bright end of our sample, which is a natural consequence of the much larger intrinsic brightness of subdwarfs and early-type main-sequence stars, and the fraction of quasar contaminants increases towards larger apparent magnitudes. It is possible to eliminate a fair fraction of the contaminants in the

photometric-only sample by using additional information such as proper motions and infrared colours (see Sect. 5.4).

3.3 Completeness of SDSS spectroscopy for DA white dwarfs

The sample produced here provides an excellent opportunity to investigate the spectroscopic completeness of SDSS for DA white dwarfs. We used the cuts in Table 1 to select both the spectroscopic and photometric objects within DR7. From these two sets of data, we then calculate the spectroscopic completeness within the $(u - g, g - r)$ colour-colour plane (Fig. 3). The upper middle and right panels display the density of spectroscopically confirmed DA white dwarfs (middle) and contaminants (such as NLHS and quasars, right hand side panel). For comparison, the upper left hand panel shows the DA white dwarf cooling tracks from Holberg & Bergeron (2006)¹. The efficiency of our colour cuts is obtained for each bin within the $(u - g, g - r)$ plane as the ratio of the number of the DA white dwarfs to the total number of objects in the bin (lower centre panel). This

¹ See <http://www.astro.umontreal.ca/~bergeron/CoolingModels> for an updated grid.

Table 2. Efficiency and completeness of the polynomial colour-colour cuts (Table 1) as a function of SDSS g magnitude. The total number of spectroscopic objects that matched our selection and were visually classified was 7444. The classification ‘Other white dwarfs’ contains white dwarfs of type DAB, DAO, DB, DC, DQ, DZ, magnetic white dwarfs and white dwarf+MS binaries. The classification ‘Other’ includes CVs, galaxies, peculiar objects and unidentified spectra. The final two right hand columns show the number of photometric-only objects in each g magnitude bin (N_{Tot}) and the number of predicted DA white dwarfs, calculated by multiplying this by the efficiency (N_{DA}). The bottom line of the table gives the total number of DA white dwarfs with ($g \leq 19$) in Eisenstein et al. (2006), and the number of them included in our colour cut.

g	All WD Candidates	DA WD N	%	NLHS N	%	QSO N	%	Other WD N	%	Other N	%	Efficiency	Completeness	Photometric-only	
														N_{Tot}	N_{DA}
≤ 16	258	79	30.6	161	62.4	0	0.0	13	5.0	5	1.9	30.6%	95.8%	893	273
16-17	581	326	56.1	185	31.8	22	3.8	44	7.6	4	0.7	56.1%	96.7%	980	550
17-18	1719	1092	63.5	225	13.1	230	13.4	165	9.6	7	0.4	63.5%	96.5%	2278	1447
18-19	4886	3139	64.2	269	5.5	1028	21.0	439	9.0	11	0.2	64.2%	95.0%	5190	3332
Total	7444	4636	62.3	840	11.3	1280	17.2	661	8.9	27	0.4	62.3%	95.5%	9341	5819
Total DA WD Photometrically selected DAs														Completeness	
Eisenstein	2889	2757												95.4%	

clearly displays a reduced efficiency of selecting both the hottest and coldest white dwarf because of the increased numbers of contaminants. Our selection method however has an extremely high efficiency when selecting white dwarfs with temperatures between $\sim 10,000 - 20,000\text{K}$. The number of DA white dwarfs without SDSS spectroscopy is predicted by scaling the number of photometric-only objects with the efficiency (resulting in the lower left panel). Finally, the DA white dwarf spectroscopic completeness was calculated as the ratio of spectroscopically confirmed DA white dwarfs to the total number of DA white dwarfs, with and without spectroscopy (lower right panel). The overall spectroscopic completeness is 44.3% down to $g = 19$. As mentioned in Sect. 3.1, this analysis is limited to white dwarfs with $T_{\text{eff}} \gtrsim 8000\text{K}$. The preference of SDSS spectroscopy to target quasars is clearly seen in the lower right corner of the spectroscopic completeness colour-colour diagram, where the vast majority of quasars lie. This corresponds to a very high spectroscopic completeness for cool DA white dwarfs. In contrast, the spectroscopic completeness for white dwarfs with $T_{\text{eff}} \gtrsim 12000\text{K}$ is significantly lower.

4 CROSS-MATCHING WITH UKIDSS

All (spectroscopic and photometric-only) objects from the DA selection in SDSS DR7 were matched with the UKIDSS database using the CrossID function. To decide upon a matching radius, a sample of 5000 randomly selected spectroscopically confirmed DA white dwarfs were matched to the UKIDSS database with a $60''$ search radius r . The distribution of the distance between the SDSS objects and the UKIDSS matches is shown in Fig. 4. The number of all possible matches within $60''$ (black histogram) grows approximately as r^2 , as would be expected for chance coincidence, whereas true matches are primarily within $r < 3''$. Selecting only the closest match (blue histogram), the majority of these random mismatches are removed. The blue and black distributions agree well at small distances ($r \lesssim 2.5''$), indicating that crowding is not a major problem. $2.5''$ is much larger than the quoted astrometric accuracies of both

Table 3. The number of all SDSS DR7 objects satisfying our constraint set (Table 1), and of various subsets with different UKIDSS bands.

Detections in band	Spectroscopic Objects	Photometric Objects
Total SDSS	7444	9341
Any UKIDSS	1990	1771
Y	1815	1614
J	1787	1549
H	1503	1281
K	1108	840
$H \& K$	1075	809
$J, H \& K$	979	720

SDSS and UKIDSS (of order a few tenths of an arc second), but the large proper motions of the white dwarfs and the potentially large (\sim few years) time interval between both surveys can lead to positional shifts up to a few arc seconds. We adopt $r = 2.5''$ for the final cross-matching of our spectroscopic and photometric-only SDSS DA samples with UKIDSS, which limits the number of spurious matches, and will exclude only a handful of (halo) objects with extremely high proper motions. Any remaining positional mismatches are flagged in the examination of the SDSS and UKIDSS images carried out later. We restrict our analysis to unresolved systems, as the physical association of spatially resolved companions to white dwarfs will be difficult to demonstrate with the available data. Consequently, objects that are flagged as partially resolved in the UKIDSS images are removed from the sample.

A total of 1990 of the SDSS objects with spectra were found to have at least one measured magnitude in the UKIDSS database. 1275 of these are spectroscopically confirmed DA white dwarfs. Similarly, 1771 of the photometric-only objects had at least one match in the UKIDSS database.

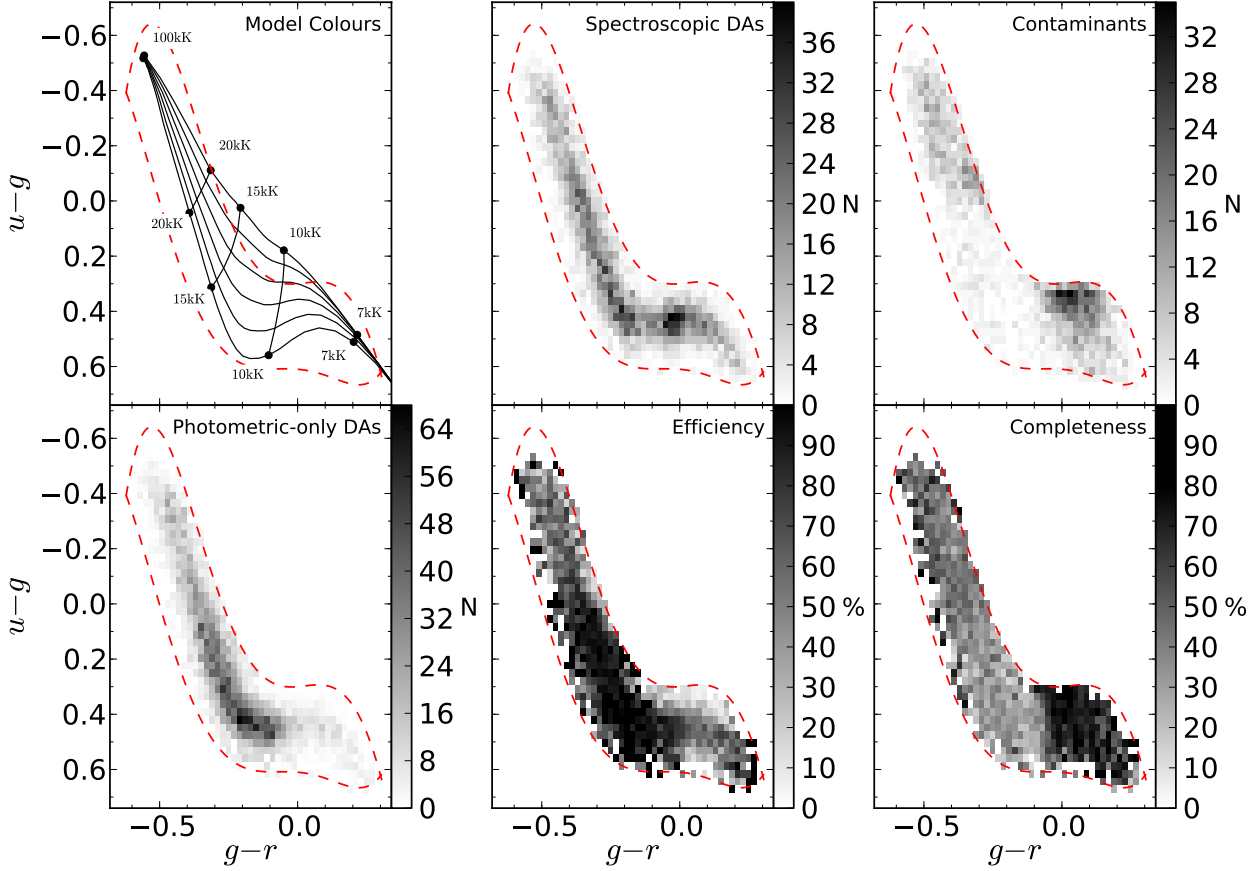


Figure 3. The spectroscopic completeness of DA white dwarfs in SDSS DR7 within the $(u - g, g - r)$ colour-colour plane. In the top left panel, the colour selection from Table 1 is shown as a red dashed line, overlaid with the DA white dwarf cooling tracks of Holberg & Bergeron (2006). From the bottom up, these curves represent $\log(g) = 7.0 - 9.5$ in steps of 0.5. The number of spectroscopically confirmed DA white dwarfs and contaminants within our colour selection are shown in the upper middle and right panels, respectively. Two distinct regions of high contamination are visible, with NLHS and quasars being concentrated at the bluest and reddest colours of the DA “banana”, respectively. The number of DA white dwarfs without SDSS spectroscopy is shown in the bottom-left panel, calculated as the number of photometric-only objects weighted by the colour-dependent efficiency of our selection algorithm (lower middle panel). Finally, the spectroscopic completeness of SDSS for DA white dwarfs, i.e. the ratio of spectroscopic DAs to the total number of DAs, is shown in the bottom right panel. Cool white dwarfs have a very high completeness thanks to their colour-proximity to ultraviolet-excess quasars, which were intensively targeted by SDSS.

5 IDENTIFYING INFRARED EXCESS OBJECTS

5.1 DA White Dwarf Fitting

A grid of synthetic DA white dwarf spectra was calculated with the model atmosphere code described by Koester (2010) and using the latest line profiles of Tremblay & Bergeron (2009). These cover $T_{\text{eff}} = 6,000 - 100,000\text{K}$ in 131 steps nearly equidistant in $\log(T_{\text{eff}})$, and $\log(g) = 5.0 - 9.5$ in steps of 0.25dex.

5.1.1 Fitting the SDSS spectroscopy

We fitted the SDSS spectra of all DA white dwarfs found within our colour cuts (Table 1) following the method described in Rebassa-Mansergas et al. (2007). A χ^2 minimisation is used to find a best fit from our grid of DA white dwarf model spectra, providing $\log(g)$ and T_{eff} . Using the cooling models of Holberg & Bergeron (2006), M_{wd} , R_{wd} and the distance d can be calculated for each object.

5.1.2 Fitting the SDSS photometry

We also fitted *all* photometric objects found with our colour cuts, including all objects that do have SDSS spectroscopy. We also fitted objects known *not* to be DA white dwarfs, to allow us to investigate the properties of the contaminants among the photometric-only DA candidates.

Photometric objects were fitted by comparing the SDSS u, g, r and i magnitudes to the white dwarf model grid, again based upon a smallest χ^2 . Model magnitudes were calculated for each of the $\log(g)$ and T_{eff} values by folding the theoretical spectra through the SDSS and UKIDSS *ugrizYJHK* filter curves. Magnitudes redder than i were not included since we are searching for composite systems. This ensures we can recognise objects with an excess already showing in z , such as white dwarf plus M-dwarf binaries. This does not significantly affect the spectroscopic fitting method because we fit line profiles. This method is most sensitive at shorter wavelengths, where the companion does not significantly contribute. For the majority of photometric DA can-

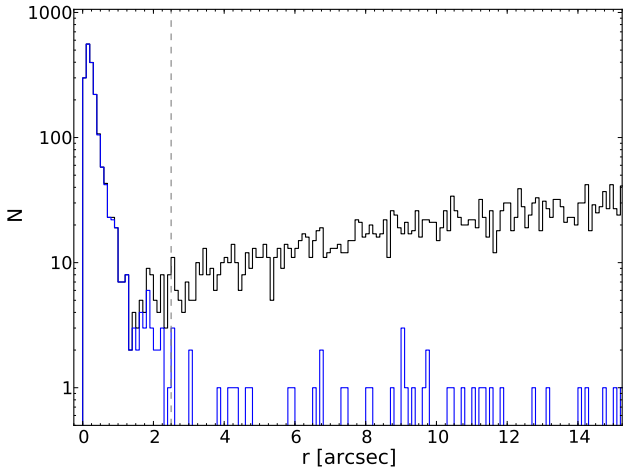


Figure 4. Spatial offsets of the SDSS and UKIDSS positions for a sample of 5000 spectroscopically confirmed DA white dwarfs randomly selected from our constraint set (Table 2). The blue histogram shows the distance to the closest neighbour in UKIDSS, the black histogram plots the distances to all possible matches. The bins have a width of $0.1''$.

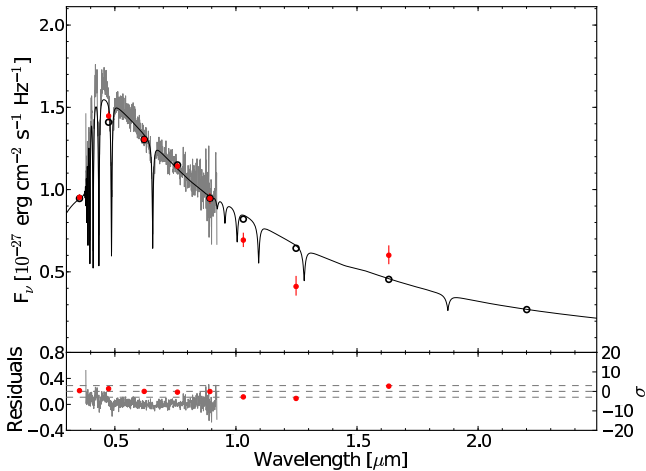


Figure 5. The SED of SDSS J1218+0042, an example of a spectroscopically confirmed DA white dwarf with a possible IR flux excess (classified as DAire: in Table 7), SDSS J1218+0042. The best-fit model to the *ugri* photometry is shown ($T_{\text{eff}} = 10000\text{K}$, $\log(g) = 7.75$), which results in an *H*-band excess just below 3σ . Adopting the slightly higher temperature ($T_{\text{eff}} = 11173\text{K}$) from the analysis of the SDSS spectrum boosts the excess to just above 3σ , flagging the object as an IR excess candidate. However, given that *Y* and *J*-band magnitudes fall significantly below the model, further IR data are necessary to confirm or refute the IR excess of this white dwarf.

didates, the 4-band photometry did not provide sufficient constraints to accurately determine the surface gravity. For objects with calculated effective temperatures in the range $9000 - 20000\text{K}$, where the spectral line widths are narrow and therefore do not significantly affect the SED, we adopted a canonical value of $\log(g) = 8.0$ for those objects.

The temperatures measured from the SDSS photometry were found to be systematically lower than those from the fitting of line profiles (e.g. Table 9; objects with SDSS spectroscopy, but fitted with the photometric method). Our

sample of SDSS white dwarfs overlaps with the Palomar Green (PG) sample, and Fig. 7 shows a comparison between our spectroscopic and photometric temperatures with those of Liebert et al. (2005), which were determined from independent data, spectral models, and fitting routines. We find good agreement between the results of Liebert et al. (2005) and our spectroscopic method. However, our photometric temperatures are systematically too low, a trend that is strongly correlated with either white dwarf temperature or distance. At 200pc (500pc), the photometric temperatures are on average 5% (10%) below our and Liebert’s spectroscopic values. This could suggest that interstellar reddening is, at least in part, the culprit for reduced temperatures. While reddening would not significantly effect the shape of the line profiles, it could noticeably change the slope of the continuum (see also Holberg et al. 2008). No clear correlation is, however, seen when comparing the mismatch in temperatures to the Schlegel et al. (1998) values of $E(B - V)$ at the positions of the white dwarfs. The Schlegel et al. maps probe interstellar reddening through the entire Galaxy, whereas the white dwarfs in our sample lie at a few hundred parsecs at most. Typical (total Schlegel) reddening along the lines-of-sight towards our white dwarfs is $E(B - V) \sim 0.05$. De-reddening the SDSS photometry with that total $E(B - V)$, and re-fitting the photometric white dwarf sample indeed leads, as expected, to a large over-correction of the white dwarf temperatures. Analysing the sample of spectroscopic DAs, we estimate that the typical reddening in front of the white dwarfs is $E(B - V) \sim 0.01 - 0.02$. However, we can not systematically correct for the effect of reddening for the sample of photometric-only DA candidates. We note that for hot white dwarfs, $T_{\text{eff}} \gtrsim 45000\text{K}$, non-LTE effects become important, which may also lead to some systematic differences in the fit parameter for the hottest stars in our sample. Therefore, the temperatures calculated from the photometry alone have an additional systematic uncertainty, on top of the statistical uncertainty from the fit, and the true temperatures are likely to be a few thousand Kelvin higher. In the context of our search for infrared flux excess (Sect. 5.2 below), changing the white dwarf temperature by a few thousand Kelvin does not have a significant impact on the level of excess detected (see Sect. 6 for examples).

5.2 IR Excess Detection

In both the spectroscopic and photometric fitting methods, the best fit model extends into the IR and all objects with UKIDSS data were examined for an excess by comparing the IR white dwarf model flux with the observed *YJHK_s* magnitudes. Objects with a 3σ excess in any band over the white dwarf model were defined as a robust excess candidate (“DAire” and “DA:ire” for the spectroscopically confirmed DAs and the photometric-only DA candidates, see Tables 7, 8 and 9). Further to this, objects that appeared to have a best fit model which over-estimated the flux in *Y*, *J* and *H*, but showed only a $\sim 2\sigma$ excess in *K* were also flagged as tentative excess candidates (“DAire:” and “DA:ire:”, as above, Tables 7, 8 and 9), see Fig. 5 for an example. Further IR data is definitely needed to confirm these marginal IR excess candidates. Similarly, spectroscopically confirmed DAs (photometric DA candidates) with close to 3σ excess that by eye

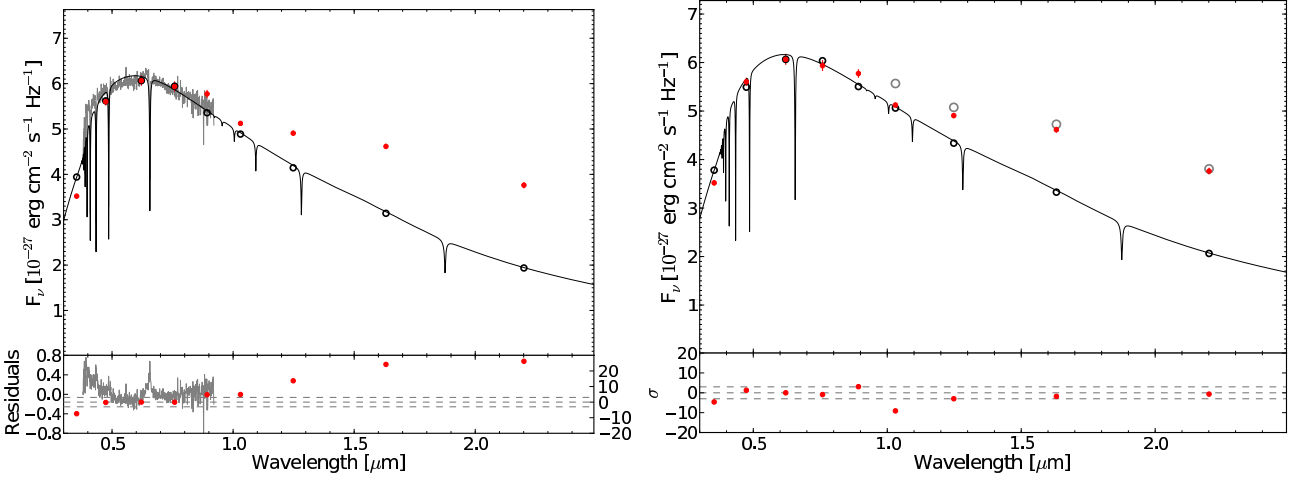


Figure 6. SDSS J0135+1445; a cool white dwarf with a probable low mass companion. The fit is a $T_{\text{eff}} = 7467 \pm 18\text{K}$, $\log(g) = 7.34 \pm 0.04$ spectra at a distance of $69 \pm 2\text{pc}$. The calculated mass is $M_{\text{wd}} = 0.29 \pm 0.01 M_{\odot}$. The photometry is best fit with a white dwarf of $T_{\text{eff}} = 8000 \pm 20_{10}\text{K}$, $\log(g) = 8.0$. Based upon the fit to the photometry, the addition of an L8-type companion to the white dwarf magnitudes is the best fit to the IR excess (Table 9) and is plotted on the right hand figure as open grey circles. The model Y-band magnitude does not match the UKIDSS Y measurement, but we found that the Y-band data did relatively often disagree with SDSS z and UKIDSS J .

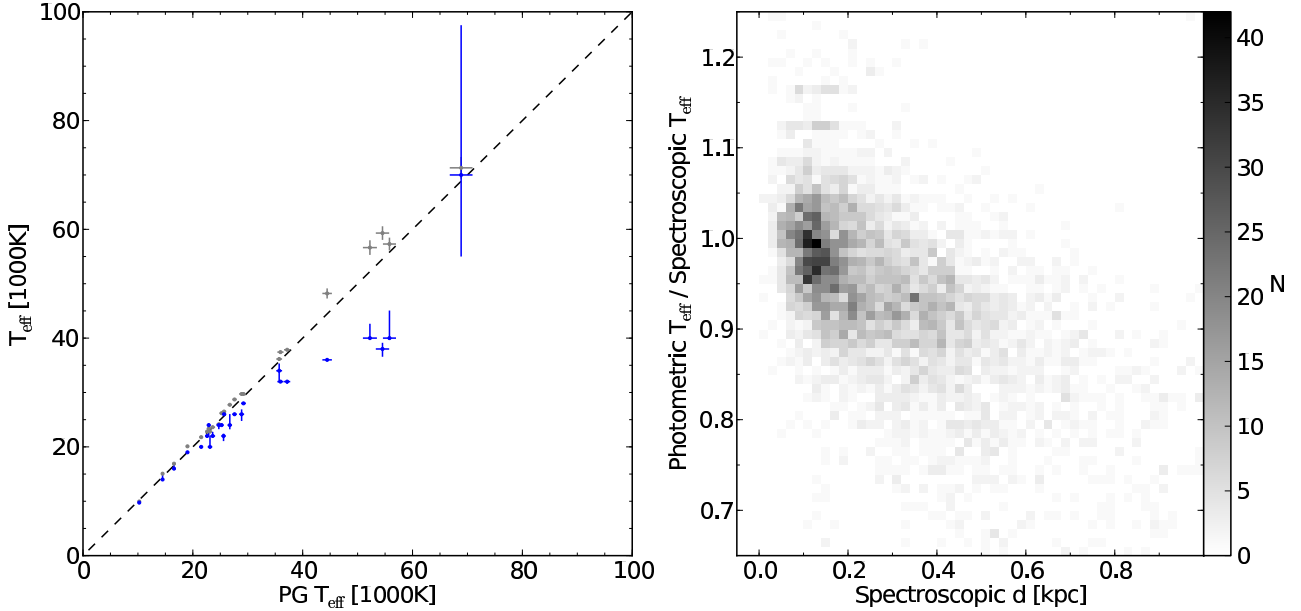


Figure 7. A demonstration of the systematically lower measured photometric effective temperatures. The left hand panel shows the Liebert et al. (2005) PG survey white dwarfs with corresponding stars in our sample (25 objects). This figure compares the effective temperature calculated by Liebert et al. (2005) with that from our spectroscopic (grey) and photometric (blue) fitting techniques. When using the photometric method, we significantly underestimate the temperature of hot white dwarfs. The hottest white dwarf at 70,000K has a large error on the photometric fit because the continuum slope of the white dwarf at these temperatures is effectively Rayleigh-Jeans and therefore contains no temperature information. In the right hand panel we show the ratio of the effective temperatures calculated using the photometric and spectroscopic fitting methods for each of the objects in the spectroscopic DA white dwarf sample, as a function of distance. Again, we underestimate the effective temperature of white dwarfs at large distances.

require further data to confirm the excess were also marked as “DAire:” (“DA:ire:”). For the photometric-only objects the uncertainty on the model parameters is generally larger compared to the spectroscopically confirmed DAs. This was accounted for by not flagging objects with a marginal IR excess *and* a large uncertainty on effective temperature as excess candidates.

Spurious excesses were often caused by spatially close background or foreground objects to the white dwarf and bad SDSS or UKIDSS images. We visually inspected all flagged sources and discounted resolved and partially resolved systems because the physical association of the two objects could not be demonstrated based on the available data.

A total of 42 white dwarfs were found to have an excess from the spectroscopic fitting method, and 105 infrared excess candidates were found from the photometric fitting method (Table 4). The excesses have a variety of spectral shapes, generally consistent with various spectral type companions. Table 7 and 8 list all the spectroscopic and photometric IR excess candidates, respectively.

5.3 IR Excess Modelling

The $YJHK_s$ magnitudes of objects that were found to exhibit an infrared excess were fitted with a composite model consisting of the best-fit white dwarf plus a set of low-mass companions with spectral types M0 through to L8. We used the 2MASS JHK_s magnitudes of Hoard et al. (2007), which we converted into the UKIDSS filter system adopting the equations given in Dye et al. (2006). Hoard et al.’s absolute magnitudes of the low-mass companions were scaled to apparent magnitudes using the distance modulus calculated from the white dwarf fit. For photometrically fitted objects, the white dwarf distance modulus was calculated as an average of the difference between the best-fit absolute magnitudes and the SDSS apparent magnitudes in each of the u , g , r and i bands. Finally, the model magnitudes of the composite system were computed from the combined white dwarf and companion star fluxes. The best composite fit to the JHK IR photometry was calculated using a least χ^2 search and subsequently confirmed by visual inspection. Fig 8 shows reduced χ^2 as a function of companion type for three white dwarfs with well constrained companions using the photometric method as an example. It was seen that a white dwarf with a good fit to the companion has a reduced $\chi^2 \lesssim 10$, an example of the corresponding SED is shown in Fig. 6. Composite fits with $\chi^2 \sim 10 - 100$ were flagged as “bad fits” and flagged as DAire: or DA:ire in Table 7 and 8, respectively, as the nature of the IR excess remains somewhat unclear (see Fig. 9 and Sect. 5.4.1). Finally, QSOs stand out because of their very high χ^2 , $\sim 100 - 1000$ (e.g. Fig. 10). A summary of companion types for each method is given in Table 4.

5.4 Comparison of the spectroscopic and photometric methods

The results from using either the spectroscopic or purely photometric methods to find IR excess can be directly compared because *all* the objects with SDSS spectra also have SDSS photometry. We discuss in the following sub-sections how well the spectroscopic and photometric method compares for genuine DA white dwarfs (Sect. 5.4.1), what can be learned from the spectroscopic contaminants that show an IR excess when fitted with the photometric method (Sect. 5.4.2, 5.4.3), and how additional information such as IR colours and proper motion could be used to suppress contaminants in the photometric-only sample (Sect. 5.4.2).

5.4.1 DA White Dwarfs

Of the 42 spectroscopic DA white dwarf IR excess candidates, 30 ($\sim 71\%$) are recovered by the photometric fitting method as well (column “DA w SIRE” in Table 4, 9 M-type,

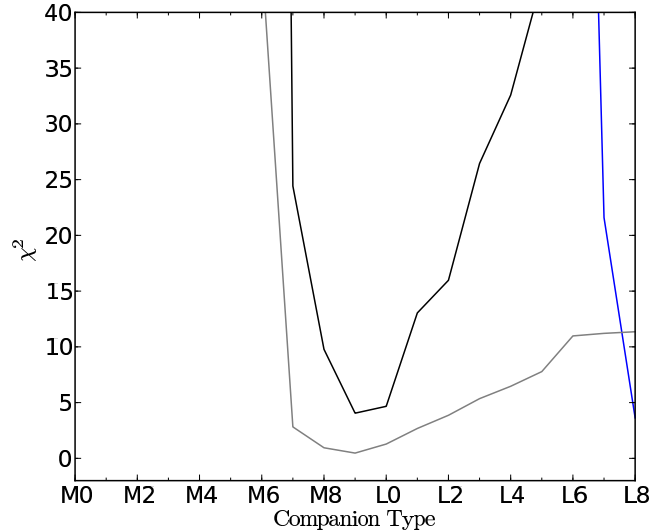


Figure 8. Reduced χ^2 as a function of companion type for three white dwarfs with well constrained companions using the photometric method. χ^2 is calculated from comparing the UKIDSS JHK magnitudes with those of the low-mass companions of Hoard et al. (2007). SDSS J0135+1145, SDSS J0842+0004 and SDSS J0925-0140 are plotted as blue, grey and black respectively. We find that a good fit has a reduced $\chi^2 \lesssim 10$, a bad fit (DAire: or DA:ire: in Tables 7 and 8) has $\chi^2 \sim 10 - 100$ and a QSO has $\chi^2 \sim 100 - 1000$.

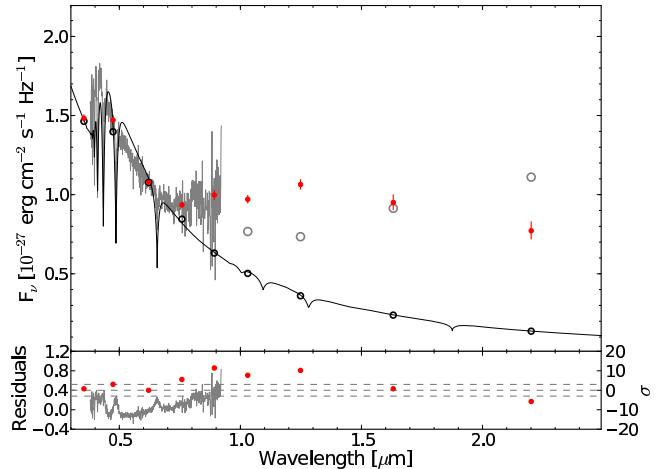


Figure 9. The SED of SDSS J1619+2533, an example of a spectroscopically confirmed DA white dwarf where the photometric method substantially underestimates the white dwarf temperature. The best fit to the spectrum is a $T_{\text{eff}} = 25595\text{K}$ and $\log(g) = 7.21$ DA white dwarf model ($M_{\text{wd}} = 0.33 \pm 0.04$), whereas the photometric fitting method finds the best solution at $T_{\text{eff}} = 18000\text{K}$ and $\log(g) = 9.5$, the latter is plotted here in black. Within the photometric method, the lower temperature (and higher gravity) leads to the distance being substantially underestimated, and therefore the flux of the companion being overestimated. Fitting the SED with the two-component model described in Sect. 5.3 compensates for the low distance by choosing a companion with a larger absolute magnitude, i.e. a later spectral type. For SDSS J1619+2533, the spectroscopic method results in a M4 type companion, the photometric method in an L6 companion. Because the optical-IR SED can not be well fitted with any companion type at the photometric distance, this object is flagged as “bad fit” in Table 9.

Table 4. Objects with an IR excess split by estimated low-mass companion type. The first column shows the IR excess candidates among the spectroscopically confirmed DAs (Table 7) and the final column contains the information on the photometric-only sample (Table 8), where there is no SDSS spectrum available for classification. The section in the middle shows all objects with SDSS spectroscopy for which fitting their *ugri* photometry resulted in an IR flux excess (Table 9), split by their spectroscopic classification. This set of objects is useful to gauge the contamination of photometric-only IR excess DA candidates by other types of objects. It also allows the like-for-like comparison of the infrared excess detection/modelling for genuine DA white dwarfs. To aid this comparison of the two methods, the column “DA (w SIRE)” lists the spectroscopically confirmed DA white dwarfs that exhibit an IR flux excess when fitted with both the spectroscopic and photometric method, and the column “DA (wo SIRE)” lists 6 spectroscopically confirmed DA white dwarfs that are found to have an IR excess only when analysed with the photometric method. A “-” mark denotes that the corresponding entry is not possible. “No Phot IR Excess” means that no photometric excess was found, even though a spectroscopic excess is seen.

	Spectroscopic			Spectroscopic using Photometric Method				Photometric	
Primary Type \Rightarrow Companion Type \Downarrow	DA	DA w SIRE	DA wo SIRE	NLHS	WDMS	DAH	QSO	Total	-
M-type	16	9	1	10	2	0	0	22	15
L-type	19	11	0	12	1	0	0	24	19
$\geq L7$ or disc	7	6	2	0	0	0	0	8	4
QSO	-	0	0	0	0	0	323	323	40
Bad fit	0	4	3	9	1	3	0	20	27
No Phot IR Excess	-	12	-	-	-	-	-	12	-
Σ	42	42	6	31	4	3	323	409	105

11 L-type, 6 $\geq L7$ -type companions/debris discs and 4 “bad fits”, which are marked as “DAire:” in Table 8), and 12 do not show an excess when using the photometric method. These 12 objects are close to the $\sim 3\sigma$ limit in the spectroscopic method and were not recovered. They were not recovered by the photometric method because of the larger uncertainty on effective temperature leading to the excesses being within the combined model and flux errors. 6 objects with DA white dwarf SDSS spectra are found to have an IR excess in the photometric method, but do not exhibit an IR excess when using the spectroscopic method (column “DA wo SIRE” in Table 4). Three of these have excesses which are accentuated by a slightly hotter photometric fit compared to the spectroscopic one. They fall just outside the criteria (Section 5.2) for having an excess in the spectroscopic method. For the other three objects the SDSS spectra are too poor to obtain reliable T_{eff} and $\log(g)$ measurements from fitting their Balmer lines. Therefore an excess was not recognised in the spectroscopic method. However, the photometric data were good enough and thus these three objects are classified as photometric IR excess candidates. We may therefore expect $\sim 9 - 17\%$ (3/36–6/36) spurious IR excess candidates from the photometric method. All objects that display an infrared excess either in the spectroscopic, or the photometric method, and have an SDSS spectrum are listed in Table 9.

Table 4 also lists the IR excess candidates split by modelled companion type. Among the 30 objects which are defined as IR excess candidates in both methods, the distribution of companion type has a similar form. $\sim 80\%$ of the companions have M or early L spectral types (split evenly between the two classes), and the remaining $\sim 20\%$ have companions $\geq L7$, i.e. brown dwarf or debris disc candidates.

As briefly outlined in Sect. 5.1, the temperatures resulting from the photometric fits are systematically too low, and this will introduce a bias in the spectral type of the

companion. The flatter SED of a cooler white dwarf will reduce/distort the IR flux excess relative to the white dwarf, and therefore a later type companion will provide sufficient flux to account for the excess. An additional effect is that a cooler white dwarf will suggest a lower distance when fitting the *ugri* magnitudes. Underestimating the distance will lead to an overestimate of the absolute flux of the companion. To compensate for this, the fit to the companion will resort to a companion with a larger absolute magnitude, i.e. lead to a companion spectral type that is too late. A moderately extreme example of these effects is shown in Fig. 9 (SDSS J1619+2533, see Table 9). Assuming that the spectroscopic fit parameters are correct, the white dwarf temperature is underestimated by $\sim 8000\text{K}$, which leads to an L6 companion in the photometric method, as opposed to an M6 companion resulting from the spectroscopic analysis. This object is marked in the notes column as having a bad fit to the companion in the photometric method, where a “bad fit” is defined as an object having an excess which is inconsistent with any companion type (at the photometric white dwarf distance).

5.4.2 Quasar Elimination

As can be seen in Table 4, a significant fraction (323) of the IR excess candidates from the photometric method with spectra are quasars. This is almost the entire population of spectroscopically confirmed quasars in the DA white dwarf sample with UKIDSS magnitudes. The remaining 5 quasars do not have sufficient IR data to show their quasar nature, but equally are not flagged as IR excess candidates. This is caused by the flat SED exhibited by QSOs (Covey et al. 2007). When modelled with a DA white dwarf, they generally have an effective temperature of $\sim 8000\text{K}$ and have an IR excess that is much higher than physically possible for an M-dwarf or brown dwarf companion at the distance of the (photometric) DA fit (e.g. Fig. 10). Because of the (appar-

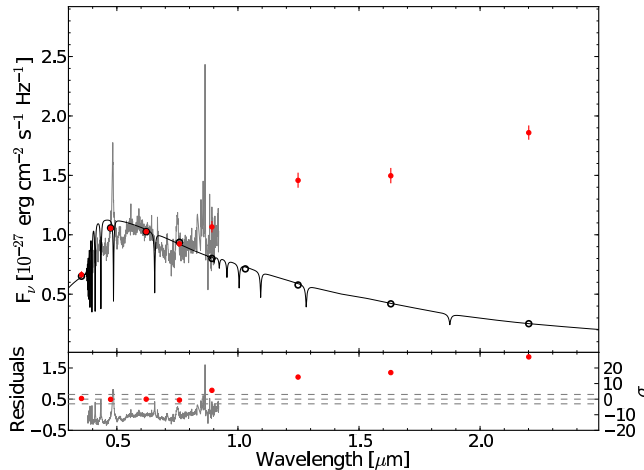


Figure 10. The SED of SDSS J0046-0044, an example of a quasar, that was selected as a candidate DA white dwarf (based on its colours, Table 1) with possible IR excess (“DA:ire:”) by the photometric method. The best-fit to the *ugri* photometry is found for $T_{\text{eff}} = 9000\text{K}$ and $\log(g) = 7.0$ at a distance of 37pc and shown as black line. The excess over the model keeps rising steeply into the mid-IR and can not be modelled by any companion type at the distance of the (photometric) DA fit, identifying this object as a quasar contaminant.

ent) low effective temperatures, the quasars also generally have low (apparent) distances. These properties, however, overlap with those of genuine cool nearby white dwarfs and cannot be used to directly distinguish between white dwarfs and quasar. Another common sign of QSOs are large jumps in brightness between adjacent magnitudes (caused by emission lines) that are not seen in any of the genuine DA white dwarfs with infrared excess. Given that we correctly classified, on the base of their optical-IR SED, 99% of (spectroscopic) quasars contaminants that were found as DA:ire by the photometric method, we are confident that we can identify the vast majority of quasars among the photometric-only sample.

Among the photometric-only sample of IR excess candidates, we find 38 objects whose SEDs are very similar to those of our 323-strong spectroscopically confirmed quasar sample and which we therefore believe to be quasars as well. Optical spectroscopy is needed to confirm their nature. These have been removed from Table 8 and can be found in the online QSO tables available via CDS.

5.4.3 Contamination by NLHS and Non-DA White Dwarfs

Contaminant NLHS and non-DA white dwarfs are more difficult to identify and remove from the photometric-only DA candidate sample, as their overall SEDs are all rather similar. Closer inspection of the SDSS spectroscopy of the NLHS and cross-checking them in Simbad suggests that a large fraction of them are subdwarf B (sdB) stars. The bulk of subdwarfs are believed to have formed in binary interactions (Han et al. 2003; Heber 2009) and therefore it is expected that a large majority will still have companions. Such companions would cause an IR flux excess over the Rayleigh-Jeans tail of the subdwarf, and it is hence likely

that our photometric-only sample of candidate DA white dwarfs with infrared excess contains a significant contamination from sdB plus low-mass companion binaries.

Given that we fit all photometric objects with DA model spectra, we may expect some imperfections in the fits to the photometric NLHS objects. Nevertheless, the detection of a near-IR flux excess over the Rayleigh-Jeans tail of the model is likely to be correct for many of the NLHS objects among the photometric sample. However, a DA fit to the photometry of a physically much larger NLHS object will dramatically underestimate its radius, and hence its distance. Consequently, fitting the companion with the composite model (Sect. 5.3) will result in a spectral type of the companion that is much too late.

From the spectroscopic sample, we find that the frequency of NLHS inside the DA colour selection (Table 1, Fig. 2) is 14.6% (Table 2), however the level of contamination is strongly magnitude-dependent. Figure 11 (left) shows the distribution of NLHS and DA white dwarfs as a function of *g*-band magnitude. The ratio of these two, and thus the expected level of contamination of the photometric-only sample, is shown in the middle panel (this assumes that the majority of quasar have been removed because of the characteristic shape of their SED). The contamination of the photometric-only DA candidate sample by NLHS drops significantly towards fainter *g* magnitudes. Subdwarfs are ~ 100 times brighter than white dwarfs and therefore apparent magnitudes of $g \sim 18 - 19$ sample distances of many kpc. This is several times the exponential scale height of the Galactic thick-disc population, and hence the number of sdBs at such large distances is relatively small. Figure 11 (right panel) shows the photometric-only IR excess candidates as a function of *g* magnitude, where we can assume that most objects with $g \lesssim 16$ are likely to be NLHS.

An additional clue on the NLHS vs DA classification of the photometric-only objects comes from their location in the $(u - g, g - r)$ colour-colour diagram (Fig. 12, bottom right panel), where the majority of the spectroscopically confirmed NLHS objects are concentrated at the blue end of the “DA” banana. We can therefore assume that NLHS are the primary contaminants of the photometric sample in this region as well (Fig. 12, top right panel).

Assuming that the distribution of NLHS contaminants is similar between the spectroscopic and photometric-only sample, we expect ~ 259 of the 1771 photometric objects to be NLHS. When fitting the photometric sample, 31 (12%) spectroscopically confirmed NLHS were found to have an IR excess (red dots in the bottom right panel of Fig. 12). Again, assuming that the contamination among the spectroscopic and photometric samples is similar, we would expect that ~ 37 (12% of 259) of our photometric DA candidates with infrared excess (DA:ire and DA:ire:) are in reality NLHS, primarily sdB stars with main sequence companions. These are still interesting in their own right (e.g. Sect. 6.3.2.1), but not the primary focus of the IR excess search (a detailed investigation of subdwarfs with main-sequence star companions will be published elsewhere, Girven et al. (2011, in prep)).

In contrast to the above discussion on NLHS, fitting non-DA white dwarfs with DA white dwarf models is likely to provide a reasonably good estimate of all system parameters, including the companion type – the downside being that on the base of photometry only, it is nearly impossible

to differentiate between DA and non-DA white dwarfs. However, based on the statistics of the Eisenstein et al. (2006), we only expect a small level of contamination by non-DA white dwarfs (Table 2).

5.4.4 Independent checks: proper motions and infrared colours

Our method of identifying infrared excess candidates follows Tremblay & Bergeron (2007), i.e. fitting model spectra to SDSS spectroscopy and photometry. In this section, we carry out an independent investigation of our sample using colour-colour diagrams, such as previously explored by e.g. Wachter et al. (2003) and Hoard et al. (2007), and test our classification of the photometric-only systems by making use of proper motions.

Figure 13 shows the distribution of the spectroscopic SDSS/UKIDSS sample in the $(z - H, H - K)$ colour-colour space (left panel). Using model white dwarf colours, it can be seen that the DA cooling sequence runs from top left to bottom right through the white dwarf group. The NLHS and DA white dwarfs are clearly separated from the quasars, which can be understood as stars are on the Rayleigh-Jeans tail in the infrared, whereas quasars follow a flatter power law (Covey et al. 2007). Therefore, as an additional test of how reliable our classification of the photometric-only quasar candidates works, we inspected the infrared colours of the photometric-only sample. Choosing an empirical cut of $H - K > 0.627$ selects 89.6% of the quasar contaminants in the spectroscopic sample. Adopting the same $H - K$ cut for the photometric-only sample flags 38 objects as quasar candidates. This includes 31 of the 38 photometric-only objects identified as quasar candidates on the base of their SED (Sect. 5.4.2 (see online QSO table), of which only 37 have both H and K measurements). In addition, two of the $H - K$ selected QSO candidates correspond to the two “weak” photometric-only quasar candidates listed in Table 8.

A third concentration of objects can be seen in Fig. 13 in the region between the DA white dwarfs and the quasars, a significant fraction of which are DA infrared excess candidates. The presence of an infrared excess over the stellar flux distribution results in a flatter spectral slope, and hence moves these objects closer to the quasar locus. On closer inspection, some white dwarfs in this region are found to be blended sources or suffer from background contamination from a nearby galaxy and therefore were not included as infrared excess candidates.

In summary, adopting $H - K > 0.627$ would efficiently remove the bulk of contaminating quasars from the photometric-only sample, however, such a cut would also remove a handful of genuine white dwarfs with the largest infrared excess emission (such as e.g. SDSS J1228+1040, see Sect. 6.1.1).

Given that white dwarfs are nearby low-luminosity objects, they are expected to exhibit larger proper motions than the more luminous NLHS, and quasars are not expected to show any significant proper motion at all. Thus, proper motions can be used to distinguish between white dwarfs and quasars in the region with $H - K > 0.627$. We have retrieved proper motions from DR7 for all objects in the SDSS/UKIDSS sample. Figure 14 (left panel) shows a

cumulative proper motion distribution for the white dwarfs, quasars and NLHSs. Based upon this, we chose a cut in proper motion of p.m. ≤ 10 mas/yr to define low proper motion objects such as quasars. In the spectroscopic sample, this cut selects 7%, 74% and 97% of the DA white dwarfs, NLHS and quasar respectively, efficiently eliminating the majority of the quasar without removing too many white dwarfs.

Figure 14 (middle panel) plots the magnitude of the proper motion as a function of $H - K$. The statistical significance of the proper motion is encoded in the size of the points, where larger points denote more significant proper motions. As expected, the spectroscopically objects classified as NLHS stars and quasars show very small proper motions, which are in most cases consistent with zero. The right hand side panel of Fig. 14 shows the location of 35 photometric-only objects classified as quasar because of the characteristic shape of their SEDs (see online QSO table) that have both $H - K$ colours and proper motions. The vast majority of these objects are contained within $H - K > 0.627$ and p.m. ≤ 10 mas/yr, corroborating our SED-based classification.

A small number of objects with $H - K > 0.627$, i.e. within the “quasar” region, display large and statistically significant proper motions (Fig. 14, middle panel). These are listed in Table 5. Among those objects are three spectroscopically confirmed DA white dwarfs. At closer inspection, the UKIDSS magnitudes of SDSS J1244+0402 may be contaminated by a nearby background object, which would lead to a spurious $H - K$ colour. The other two spectroscopic DA white dwarfs, SDSS J0753+2447 and SDSS J1557+0916 have very red $H - K$ colours and high proper motions. They are therefore excellent IR excess candidates. Applying the same procedure to the photometric-only DA candidate sample, SDSS J0959+0200 is the strongest infrared excess candidate among the three photometric-only objects. SDSS J1440+1223 and SDSS J1509+0539 also appear to suffer from background contamination.

Another four spectroscopic objects with quasar-like IR colours and high proper motions are classified as three magnetic white dwarfs (DAH) and one DZ white dwarf. We would expect that the IR spectra of all of these objects should be close to a Rayleigh-Jeans distribution, suggesting that the inferred IR excess is probably real. In fact, one of the DAH, SDSS J1212+0136 is a well-studied DAH plus brown dwarf binary (Schmidt et al. 2005), which exhibits a genuine infrared excess (Debes et al. 2006) (see Sect. 6.1.3). As discussed in the introduction, the metals seen in DAZ white dwarf atmospheres are from recent or ongoing accretion (e.g. Dupuis et al. 1993; Koester & Wilken 2006). The same is true for cool DZ white dwarfs (e.g. Aannestad et al. 1993), and Farihi et al. (2010) discuss the potential connection between the large number of DZ white dwarfs, and the DAZ white dwarfs with dusty debris discs thought to originate from the tidal disruption of rocky asteroids. The DZ found here, SDSS J1342+0522, exhibits a very red $H - K$ colour. The excess in K over the model spectrum is slightly under 3σ and therefore is, in our classification scheme, only a marginal candidate for having an IR excess. This DZ white dwarf and the two new DAH white dwarfs IR excess candidates warrant further investigation.

Finally, eight quasars have statistically significant

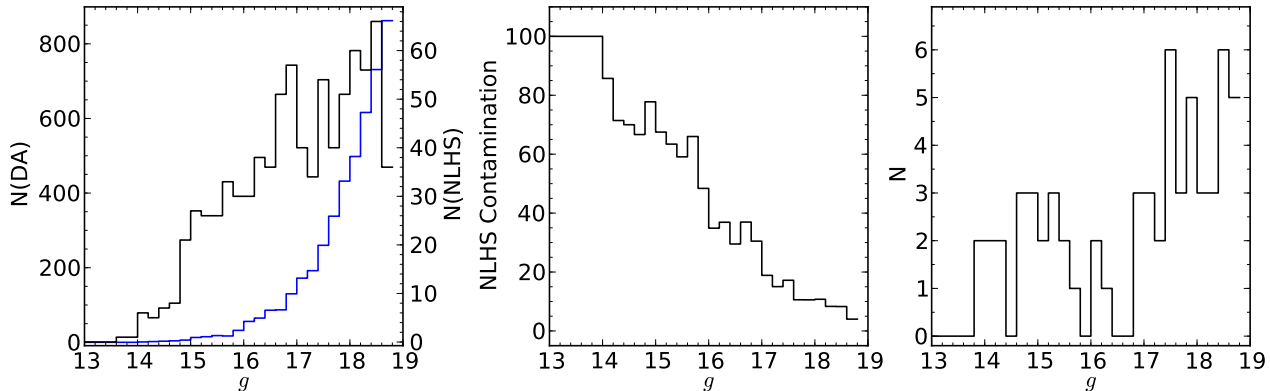


Figure 11. Left panel: The distribution of DA white dwarfs (blue, left hand scale) and NLHS (black, right hand scale) as a function of g -band magnitude. Middle panel: the fraction of NLHS as a function of g -band magnitude. The probability of contamination by NLHS clearly drops with increasing g -band magnitude. Right panel: distribution of the photometric-only IR excess candidates, the brightest of these group are most likely NLHS rather than DA white dwarfs.

proper motions ($\sim 3 - 5\sigma$; see Table 5), which highlights the fact that the SDSS vs USNO-B proper motions have to be considered with a pinch of salt: among a total of 328 quasars with SDSS spectra and UKIDSS data, we would expect only one to have a 3σ significant proper motion, and none at 4σ .

We conclude that dissecting the white dwarf sample selected with our constraint set (Table 1) using colour-colour diagrams and proper motions leads to mutually consistent results when compared to our primary methodology (Sect. 5.1- 5.3), but the spectroscopic modelling provides an additional wealth of information.

5.5 Overall Numbers

A summary of the numbers of objects at each stage of the analysis is given in Table 6. The total numbers of white dwarfs with near-IR excess are broken down according to the spectral type of their companions in Table 4.

We find that 3.3% (42 of 1275) of the SDSS spectroscopically confirmed DA white dwarfs with at least one of the $YJHK$ UKIDSS magnitudes have an IR excess and are therefore candidates for having a companion or a debris disc. However, this does not take account of the fact that the sample of white dwarfs is incomplete even within UKIDSS DR8 because for many only subsets of the IR magnitudes are available. Thus we are limited by UKIDSS coverage and the real number is higher. 2.0% of the spectroscopic DA white dwarfs are candidates for having a companion of type L0 or later, i.e. have brown dwarf companions. Similarly, 0.5% are promising disc candidates, having an excess compatible with a companion type of L7 or later. If we only discuss the objects with a detection in the K-band (required for detecting a disk), 1.2% are disk candidates, and only including objects where we are confident of the IR excess (not “DAire:” in Table 7; see Section 5.2 and 5.3), a lower limit of 0.8% of DA white dwarfs have a brown dwarf companion.

For the photometric-only sample, where we have fitted the SDSS and UKIDSS photometry, 5.9% are IR excess candidates. However, this number will be affected by the efficiency of white dwarf selection (62.3%) and the efficiency of removing contaminants. Assuming that we remove

Table 5. Objects with quasar-like infrared colours ($H - K \geq 0.627$), but large ($\geq 10\text{mas/yr}$) and statistically significant ($> 3\sigma$) proper motions. The significance of the proper motions is listed as $\sigma_{\text{p.m.}}$. Classifications are given for the objects that have SDSS spectra. The comment “BG object” refers to a second resolved source being seen in the UKIDSS images. These are most likely background galaxies which would significantly affect the $H - K$ colour. For full coordinates, refer to the online spectroscopic and photometric-only tables available via CDS.

Name	$H - K$	p.m. (mas/yr)	$\sigma_{\text{p.m.}}$	Class	Comment
0043+0005	0.79 ± 0.06	13.68 ± 3.06	4.5	QSO	
0753+2447	0.64 ± 0.24	32.16 ± 3.20	10.0	DA	
0858+0938	0.88 ± 0.03	13.13 ± 3.01	4.4	QSO	
0959-0200	0.65 ± 0.15	30.25 ± 3.10	9.8	-	
1031+0341	1.05 ± 0.08	12.25 ± 3.92	3.1	QSO	
1142+1347	1.02 ± 0.05	10.10 ± 2.81	3.6	QSO	
1212+0136	1.00 ± 0.06	69.19 ± 3.21	21.6	DAH	(1)
1244+0402	0.88 ± 0.17	11.80 ± 3.09	3.8	DA	BG object
1250+1549	1.49 ± 0.02	93.14 ± 3.12	29.9	DAH	
1342+0522	0.64 ± 0.27	51.53 ± 3.24	15.9	DZ	
1427-0054	0.68 ± 0.04	15.99 ± 3.25	4.9	QSO	
1440+1223	1.43 ± 0.08	88.83 ± 2.65	33.5	-	BG object
1443+0910	0.96 ± 0.02	12.46 ± 2.98	4.2	QSO	
1509+0539	0.98 ± 0.25	48.29 ± 3.07	15.7	-	BG object
1514+0744	0.76 ± 0.07	102.64 ± 5.06	20.3	DAH	
1553+0718	0.80 ± 0.01	14.64 ± 2.75	5.3	QSO	
1557+0916	0.70 ± 0.21	25.48 ± 2.85	8.9	DA	
1557+2646	0.84 ± 0.04	10.07 ± 3.21	3.1	QSO	

(1) A magnetic cataclysmic variable in a low state (Schmidt et al. 2005; Debes et al. 2006; Burleigh et al. 2006; Farihi et al. 2008; Howell et al. 2008; Linnell et al. 2010).

all the obvious photometric-only quasar contaminants (38, see online QSO table) from the IR excess objects, the remaining 67 photometric-only IR excess candidates will be either DA white dwarfs or NLHS. As discussed previously, we estimate that ~ 37 of these are NLHS (Section 5.4.3). This number is very similar to the amount of “bad fits” found in from the photometric method and so we believe the majority of “bad fits” come about from NLHS contaminants in the photometric-only sample. Therefore, we expect ~ 30 (2.7% of ~ 1103) genuine DA white dwarfs with IR

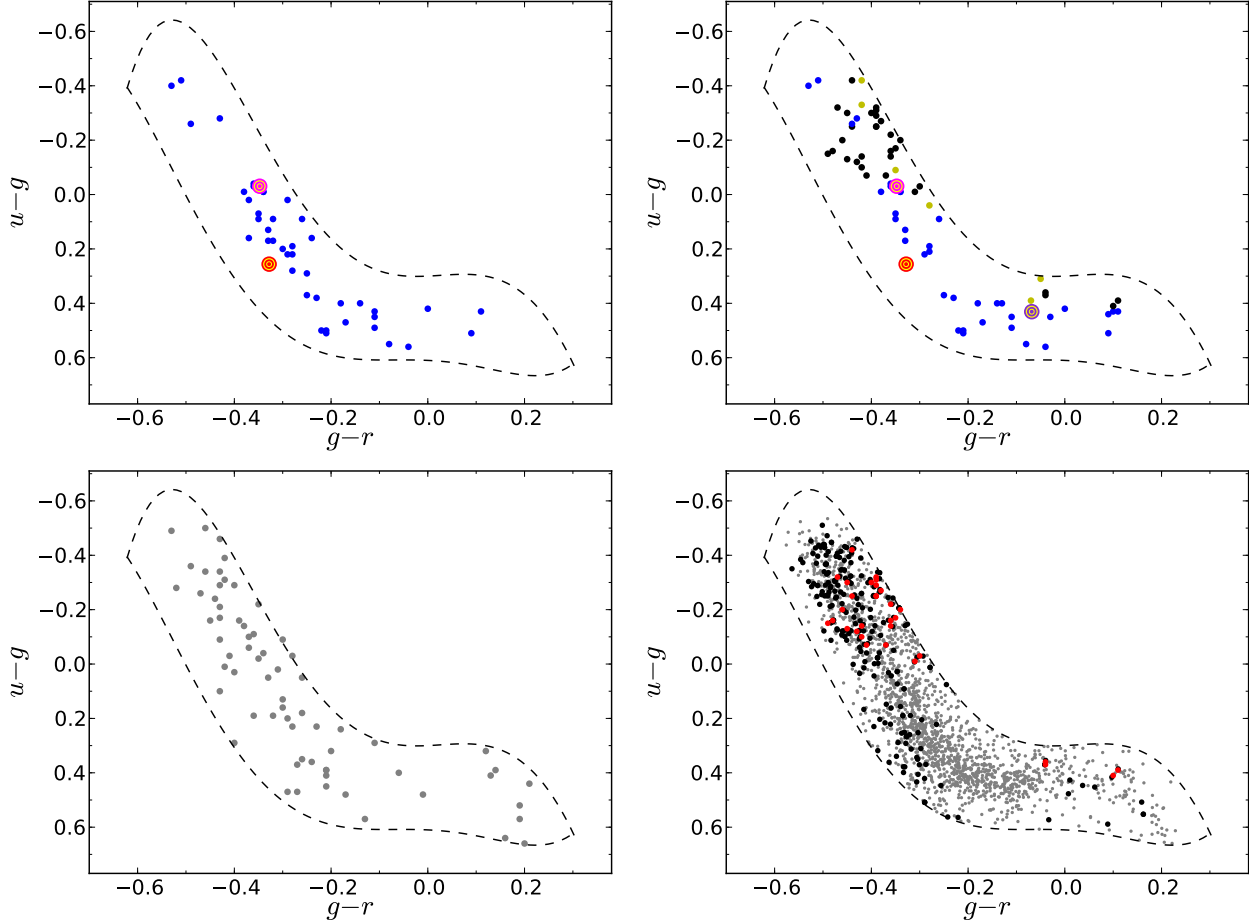


Figure 12. Top left panel: the distribution of the 42 spectroscopically confirmed DA white dwarfs with infrared excess (Table 7) in the $(u - g, g - r)$ colour-colour space. The black dashed line outlines the $(u - g, g - r)$ DA colour selection (Table 1, fig. 2). Top right panel: the distribution of the 74 IR excess objects found by photometric method (excluding quasars and quasar candidates), with DA white dwarfs, non-DA white dwarfs and NLHS shown in blue, yellow, and black respectively. SDSS J1228+1040 and SDSS J1043+0855, two DA white dwarfs known to have debris discs, are indicated by pink and red bulls-eye symbols, respectively (top left and right panel, see Sect. 6.1.1, 6.1.2). SDSS J1212+0136, a known magnetic white dwarf with a brown dwarf companion is shown as purple bulls-eye symbol (right panel only, see Sect. 6.1.3). Bottom left panel: the distribution of the 67 photometric-only infrared excess candidates. Bottom right panel: all photometric-only objects satisfying our DA constraint set from Table 1 (1771 objects, gray dots), spectroscopically classified NLHS (209 objects, black), and spectroscopically classified NLHS with an infrared excess (31 objects, red). Based on the analysis of the spectroscopic sample (Sect. 5.4.3), we estimate that $\sim 12\%$ of the photometric-only objects are NLHS, with a strong concentration towards the (blue) top-end of the DA “banana”.

excess among the photometric-only DA white dwarf candidates. These infrared excess candidates show a similar distribution in companion type when compared to the spectroscopic sample. Considering only the objects we are confident of the excess (not “DA:ire:” in Table 8; see Section 5.2 and 5.3), 1.8% (19) of the photometric-only DA white dwarf candidates are likely to have a brown dwarf companion.

6 NOTES ON INDIVIDUAL OBJECTS

Some objects of particular interest identified in the SDSS / UKIDSS cross-correlation are discussed below. We separate those into objects already known to host a disc or companion (Section 6.1), notable objects from the spectroscopic sample (Section 6.2), and the same from the photometric-only sample (Section 6.3).

6.1 Prototypical White Dwarfs

Our spectroscopic sample contains two white dwarfs that were known to host debris discs and one magnetic white dwarf with a substellar companion, and they serve hence as a benchmark for our selection procedures.

6.1.1 SDSS J1228+1040

SDSS J1228+1040 is one of two DA white dwarfs in our SDSS/UKIDSS sample known to have a debris disc. The disc was initially identified because of the highly unusual emission lines of the Ca II 8200 Å triplet (Gänsicke et al. 2006b), whose double-peaked shaped can only be explained by metal-rich gas orbiting the white dwarf within its tidal disruption radius (Gänsicke et al. 2006b). Near- and mid-IR observations revealed a substantial infrared excess over

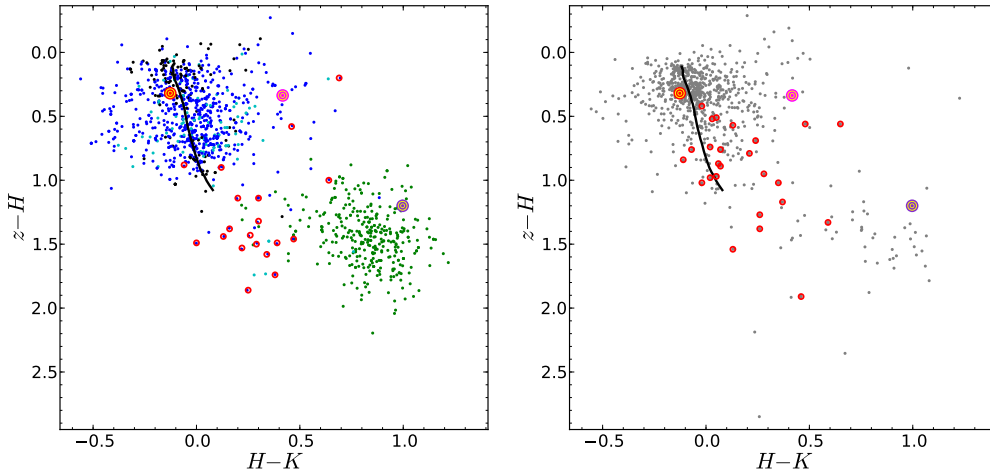


Figure 13. Location of the SDSS/UKIDSS sample in $(z-H, H-K)$ colour space. The left panel shows the objects with SDSS spectra, DA white dwarfs, NLHS, other white dwarfs and quasars in blue, black, cyan and green, respectively. The 23 robust “DAire” infrared excess objects from Table 7 are shown as red open circles. The positions of, SDSS J1228+1040, SDSS J1043+0855 and SDSS J1212+0136, two white dwarfs in the sample known to have a debris disc and a DAH white dwarf plus brown dwarf binary (see Sect 6.1.1, 6.1.2, 6.1.3), are indicated by pink, red and purple bulls-eye symbols, respectively. A track of model DA white dwarf colours for $6000\text{K} \leq T_{\text{eff}} \leq 100000\text{K}$ and $\log(g) = 8.0$ is plotted as a solid black line. High temperature white dwarfs are found at the top left end of the line. The scatter about this line cannot be explained by a spread in $\log(g)$ alone, but by uncertainties on the magnitudes (primarily those from UKIDSS) and background contamination. The photometric-only objects are shown in the right hand panel, with the 29 robust “DA:ire” infrared excess candidates (Table 8) again highlighted in red.

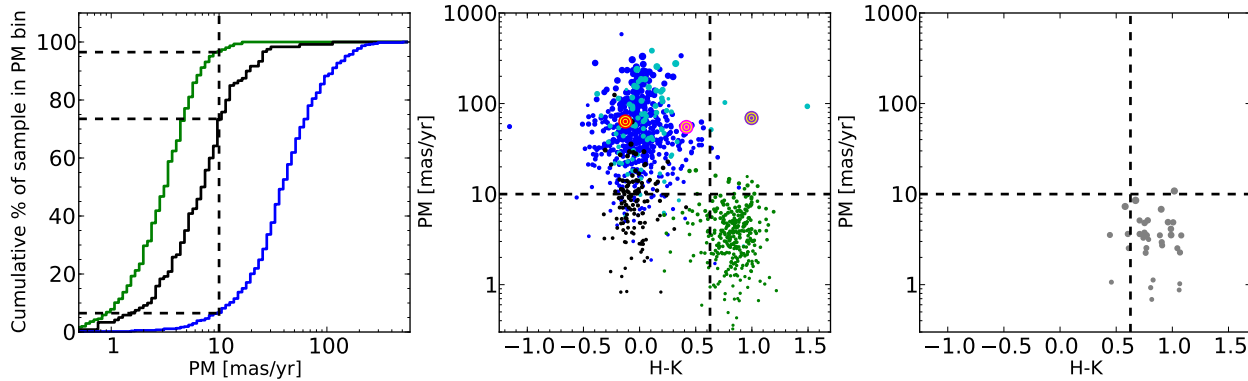


Figure 14. Left panel: The cumulative histogram of spectroscopically confirmed DA white dwarfs (blue), NLHS (black) and quasar (green) as a function of proper motion (PM). Black dashed lines show a proper motion of 10mas/yr and corresponding population levels. 7% of DA white dwarfs are contained within the bin of $\text{PM} \leq 10\text{mas/yr}$. Similarly, 74% of NLHS and 97% of quasar. Middle panel: distribution of proper motions as a function of $H-K$ colour, using the same colour-coding, and showing in addition non-DA white dwarfs in cyan. The significance of the proper motion is encoded in the size of the points, where larger points denote more significant proper motions, clipped at a maximum of 30σ . Black dashed lines show $\text{PM} = 10\text{mas/yr}$ and $H-K = 0.627$. The position of the three benchmark objects SDSS J1228+1040, SDSS J1043+0855 and SDSS J1212+0136 (see Sect 6.1.1, 6.1.2, 6.1.3) are indicated by pink, red and purple bulls-eye symbols respectively. Right panel: same as the middle panel, but showing the (35) quasar candidates identified on the basis of their SED shape (see online QSO table) which have both H and K band data in UKIDSS and proper motions in SDSS DR7.

the white dwarf, unambiguously identifying a dusty component of the debris disc, in addition to the gaseous one (Brinkworth et al. 2009). Our fits to the SDSS spectroscopy and photometry are shown in Fig. 15. The two fits differ in T_{eff} by 2000 K. However, this has very little effect on the extrapolated infrared magnitudes of the white dwarf, and the object shows a 3σ excess in H and 12σ in K , independent of the method used for fitting. At the temperature of SDSS J1228+1040, $\log(g)$ is not well constrained from fitting the $ugri$ photometry alone, however, this primarily effects

the widths of the hydrogen lines, and has a negligible effect on the spectral slope of the white dwarf model. This demonstrates that the detection of a genuine infrared excess is robust and independent of whether an optical spectrum is available.

Taking the infrared measurements at face value and ignoring our knowledge about this star, we have modelled the SDSS/UKIDSS spectral energy distribution as a white dwarf plus low-mass companion, which results in a most likely spectral type of $\geq \text{L6}$ for the companion. Based on the

Table 6. Summary of numbers at each stage of the processing. The columns are split for the spectroscopic and photometric methods. The spectroscopic sample is also further split by the classification of the optical spectra.

Constraint	Spectroscopic Objects	Photometric-only Objects
Objects Satisfying SDSS Colour Cuts	7444	9341
Spectroscopically Confirmed		
DA white dwarfs	4636	
QSO	1280	
NLHS	840	
Other white dwarfs	661	
Other Objects	27	
Objects cross matched with UKIDSS with detection in any of Y , J , H or K	1990	1771
Spectroscopically Confirmed		
DA white dwarfs	1275	
QSO	328	
NLHS	209	
Other white dwarfs	172	
Other Objects	6	
Objects with Detections in H & K	1075	809
K	1108	840
Spectroscopically Confirmed		
DA white dwarfs	571	
QSO	316	
NLHS	124	
Other white dwarfs	94	
Other Objects	3	
IR Excess Objects	42	105

SDSS/UKIDSS data alone, it is impossible to distinguish between a low-mass companion and a dusty disc, but mid-infrared data can break this degeneracy. We therefore classify infrared excess candidates that require a companion later than L7–8 as brown dwarf / dusty debris disc candidates

SDSS J1228+1040 exhibits a very red $H - K$ colour in the ($z - H$, $H - K$) colour-colour diagram shown in Fig. 13, where it is clearly separated from the white dwarf model sequence. This region of the colour-colour space is therefore likely to harbour white dwarfs with a strong K -band excess. A significant number of the IR excess candidates in Sect. 5.2 also lie in this region, as well as somewhat below (corresponding to a H and K -band excess). SDSS J1228+1040 is also prominent in Fig. 14 thanks to its relatively high proper motion and red $H - K$ colour. In summary, it is encouraging that this benchmark system indeed stands out in the various diagnostics we have considered.

6.1.2 SDSS J1043+0855

SDSS J1043+0855 is the second white dwarf in our sample known to have a gaseous debris disc (Gänsicke et al. 2007), though the evidence for an infrared excess in the

near- and mid-IR is marginal (Melis et al. 2010, Brinkworth et al. 2011, in prep.). Based on the published results on this object, we would not expect to detect any excess in the UKIDSS photometry. In our analysis of the SDSS spectrum, we find $T_{\text{eff}} = 17912 \pm 360$ K and $\log(g) = 8.07 \pm 0.08$, consistent within the errors with the parameters in Gänsicke et al. (2007). The corresponding model is an excellent fit to both the SDSS and UKIDSS photometry, with no detection of an IR excess in any of the near-IR bands (Fig. 16). Adopting the K_s flux from Melis et al. (2010) rather than the UKIDSS measurement gives a 2σ excess above our model, which would again not classify as an IR excess candidate within our classification scheme (Sect. 5.2). This conclusion is confirmed by the fact that SDSS J1043+0855 falls very close to the model white dwarf sequence in Fig. 13. This system is an example where there either is no dusty disc, or where the dusty disc is too faint, e.g. edge-on, to be detected in the near-IR.

6.1.3 SDSS J1212+0136

SDSS J1212+0136 is one of three magnetic (DAH) white dwarfs that were selected by our colour cut (Table 1) and that, when fitting their $ugri$ photometry, show a substantial IR flux excess (Fig. 17, Sect. 5.4.3). This white dwarf was first reported to have a magnetic field of $\simeq 13$ MG by Schmidt et al. (2003). Schmidt et al. (2005) subsequently detected a weak $H\alpha$ emission line, from which they measured an orbital period of ~ 90 min. Based on the J band magnitude of SDSS J1212+0136, Schmidt et al. (2005) concluded that the companion to the white dwarf is a brown dwarf. Additional studies in the near-IR confirmed the brown dwarf to have a spectral type in the range L5–L8, and detected variable cyclotron emission, indicative of ongoing accretion onto the magnetic white dwarf (Debes et al. 2006; Farihi et al. 2008; Howell et al. 2008). Observations at blue and ultraviolet wavelengths show a quasi-sinusoidal flux modulation interpreted as emission from an accretion-heated polecap (Burleigh et al. 2006; Linnell et al. 2010) which is typical of strongly magnetic cataclysmic variables (Gänsicke et al. 1995; Araujo-Betancor et al. 2005; Gänsicke et al. 2006a). Despite the fact that no state of high accretion activity has been observed in SDSS J1212+0136, all observational evidence suggests that is nearly a twin of the prototypical magnetic cataclysmic variable EF Eri (e.g. Beuermann et al. 2000).

Taken on its own, the very red $H - K$ colour of SDSS J1212+0136 would suggest it to be a quasar (Sect. 5.4.2, Fig. 13). However, its stellar nature is confirmed by the detection of a significant and large proper motion (Fig. 14). Recovering this DAH white dwarf with a brown dwarf companion shows that our methods to identify DA white dwarfs with IR-excess are sufficiently robust to also find non-DA white dwarfs with genuine IR excess.

6.2 Example Spectroscopic IR Excess Candidates

6.2.1 SDSS J0135+1445

SDSS J0135+1445 is a clear candidate for being a cool white dwarf with a late-type stellar companion or brown dwarf. An excess is seen to extend over all the UKIDSS bands in

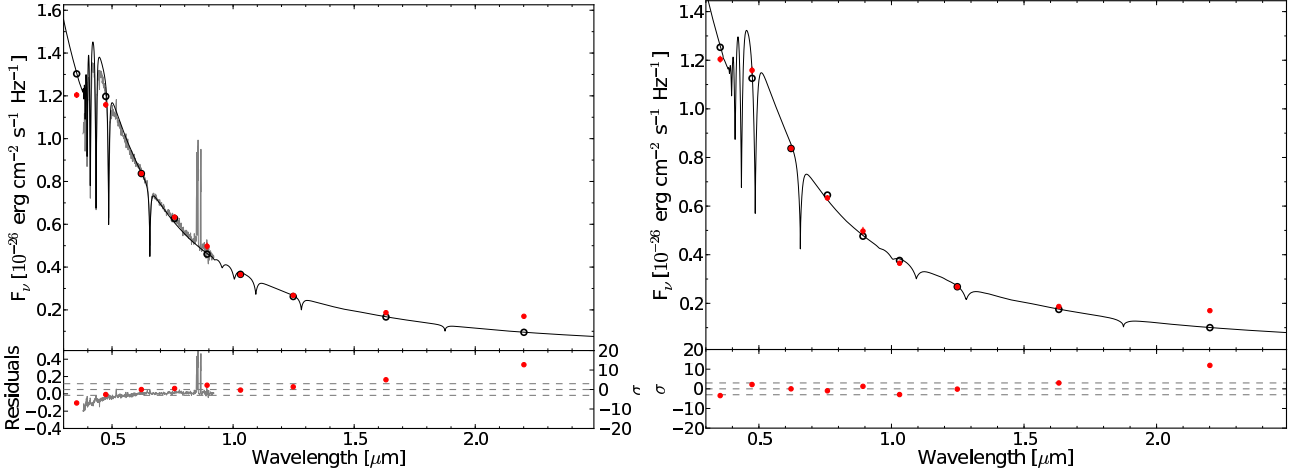


Figure 15. SDSS J1228+1040 is one of two DA white dwarfs in our SDSS/UKIDSS sample that are known to have a gaseous debris disc (Gänsicke et al. 2006b). It also exhibits a substantial infrared excess in VLT/ISAAC and *Spitzer* observations (Brinkworth et al. 2009), and hence serves as a general benchmark for our method. Fitting the SDSS spectrum (left panel) results in $T_{\text{eff}} = 22037 \pm 199\text{K}$, $\log(g) = 8.19 \pm 0.04$, implying $M_{\text{wd}} = 0.74 \pm 0.02 M_{\odot}$, and a distance of $134 \pm 3\text{pc}$, consistent with the parameters derived by Gänsicke et al. (2006b). The SDSS spectrum is shown in gray, the best-fit model in black, observed *ugrizYJHK* fluxes in red, and model fluxes in these bands as black circles. The lower panel shows the residuals from the fit (in flux units on the left axis, and statistical significance on the right axis). The corresponding fit to the *ugri* photometry gives a somewhat lower temperature, $T_{\text{eff}} = 20000 \pm 10^{10}\text{K}$, $\log(g) = 8.5 \pm 0.03^{13}\text{K}$, which has no noticeable effect on the detection of the infrared excess (right panel).

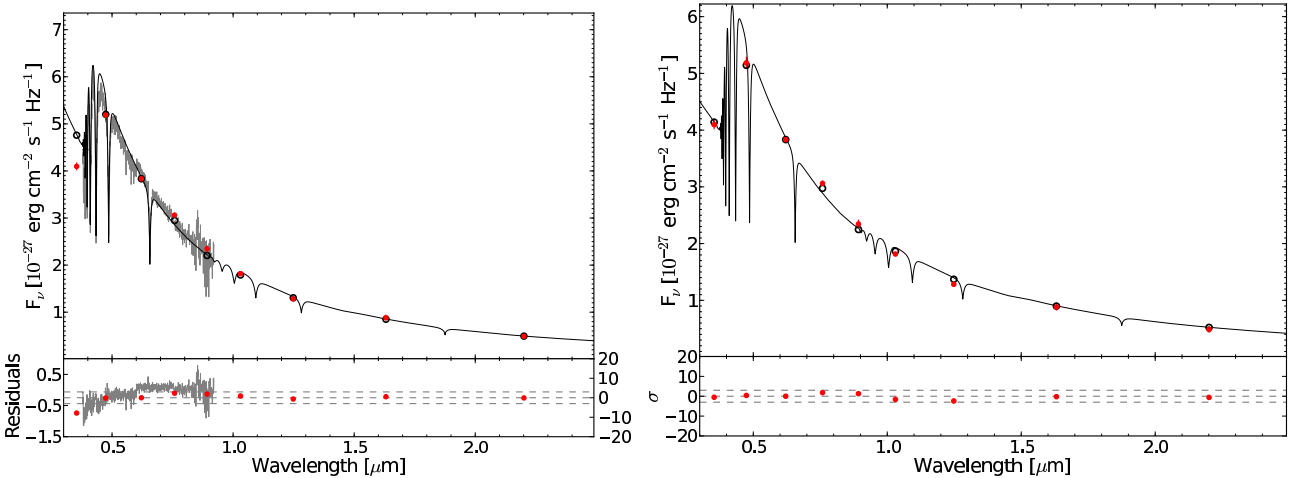


Figure 16. SDSS J1043+0855 is the second of only two DA white dwarfs in our SDSS/UKIDSS sample that is known to have a dusty debris disc. This object was discovered through optical Ca emission (Gänsicke et al. 2007) and has at best a marginal flux excess in the *Spitzer* mid-IR (Melis et al. 2010, Brinkworth et al. 2011, in prep.). Fitting the SDSS spectrum results in $T_{\text{eff}} = 17912 \pm 360\text{K}$, $\log(g) = 8.07 \pm 0.08$, the corresponding fit to the *ugriz* photometry results in $T_{\text{eff}} = 16000 \pm 10^{170}\text{K}$, $\log(g) = 7.5 \pm 0.42^{100}\text{K}$ (right panel). No IR excess is detected in the near-IR using either method, consistent with the inconspicuous location of SDSS J1043+0855 in the ($z - H$, $H - K$) and proper motion vs $H - K$ diagrams (Figs. 13 and 14, respectively).

Fig. 6. Modelling of the companion suggests that its spectral type is between L7 and L8. Spectral fitting implies a white dwarf of $T_{\text{eff}} = 7467 \pm 18\text{K}$ at a distance of $69 \pm 2\text{pc}$. A $T_{\text{eff}} = 8000 \pm 20^{10}\text{K}$ is calculated from fitting of the photometry, broadly similar to the recently discovered (resolved) DA plus brown dwarf binary PHL 5038 (Steele et al. 2009).

6.2.2 SDSS J0753+2447

SDSS J0753+2447 is a very strong candidate for being a DA white dwarf with a late-type brown dwarf or debris disc (Fig. 18). The fit to the SDSS spectrum implies a $T_{\text{eff}} =$

$13432 \pm 710\text{K}$, $\log(g) = 7.81 \pm 0.15$, with an implied distance $d = 349 \pm 32\text{pc}$ and white dwarf mass $M_{\text{wd}} = 0.50 \pm 0.08 M_{\odot}$. Fitting of the companion type was inconclusive, but the shape of the SED is similar to that of the benchmark object, SDSS J1228+1040. Therefore SDSS J0753+2447 is classified as a brown dwarf or disc candidate.

6.2.3 SDSS J1247+1035

SDSS J1247+1035 is a candidate for having a brown dwarf companion or dusty debris disc, however the UKIDSS *K*-band is only in excess by $\sim 3\sigma$ over the white dwarf model.

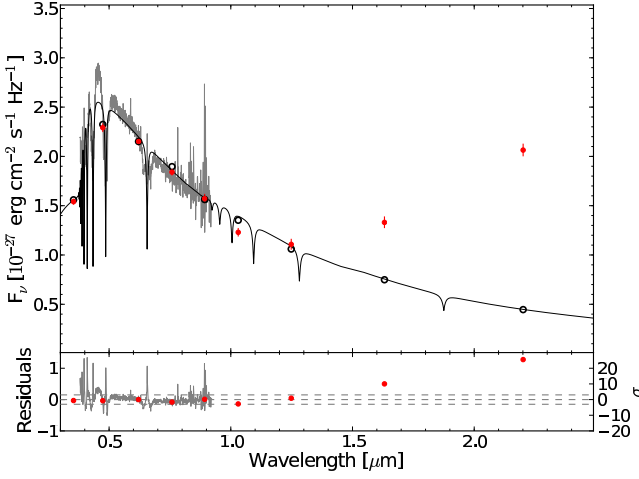


Figure 17. SDSS J1212+0136, a short-period binary containing a magnetic DA(H) white dwarf plus a brown dwarf companion (Schmidt et al. 2005). The system is undergoing weak mass transfer, producing cyclotron emission that contributes to the observed near-IR excess (Debes et al. 2006; Burleigh et al. 2006; Farihi et al. 2008). SDSS J1212+0136 was picked up by our fit to all the photometric objects satisfying the colour cuts designed to find DA white dwarfs (Table 1).

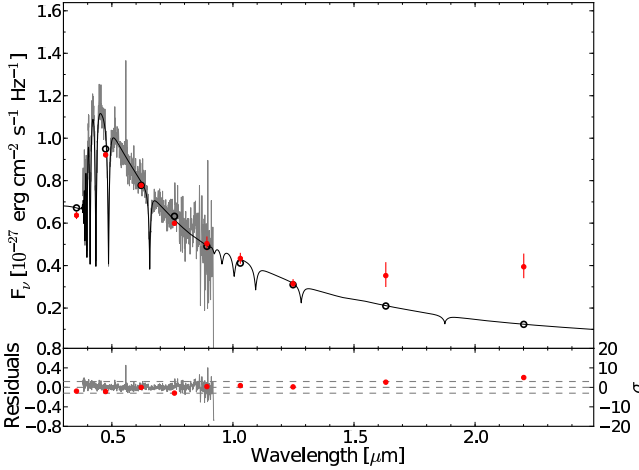


Figure 18. SDSS J0753+2447, a DA white dwarf plus dusty disc or low-mass companion candidate. The best-fit to the SDSS spectrum (black line) gives $T_{\text{eff}} = 13432 \pm 710\text{K}$ and $\log(g) = 7.81 \pm 0.15$ at a distance of $349 \pm 32\text{pc}$. The implied mass of the white dwarf is $0.50 \pm 0.08M_{\odot}$. Fitting of the 4σ K -band excess with main sequence star models proved inconclusive, however, considering the similarity to SDSS 1228+1040 (Fig. 15), this is an excellent candidate for having a brown dwarf companion or debris disc. Fitting the $ugri$ photometry leads to $T_{\text{eff}} = 12000^{+1130}_{-290}\text{K}$ and $\log(g) = 7.75^{+0.45}_{-0.41}$ at 327^{+18}_{-14}pc , with no change to the conclusions as to the nature of the excess.

Far-IR photometry of the object is required to confirm the IR excess.

6.2.4 SDSS J1557+0916

UKIDSS photometry of SDSS J1557+0916 shows a 4σ K band excess for both the spectroscopic and photometric fitting methods. The spectroscopy and photometric T_{eff} differ

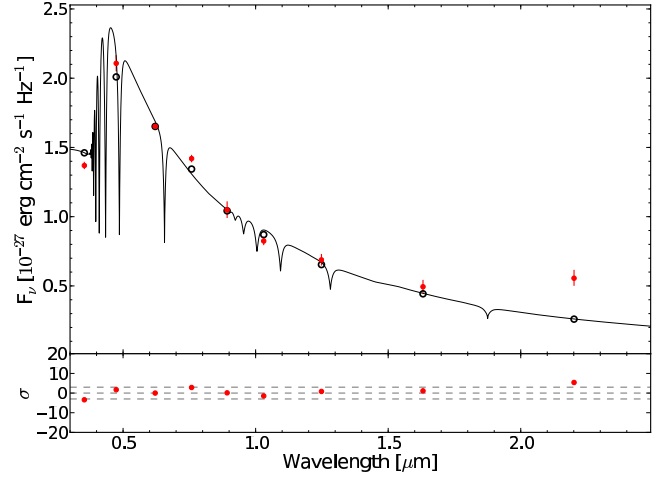


Figure 19. SDSS J0959-0200, a photometric-only DA white dwarf candidate ($T_{\text{eff}} = 12000^{+1160}_{-500}\text{K}$, $\log(g) = 8.00^{+1.20}_{-0.55}$) that exhibits a strong K -band excess, making it a strong candidate for having either a late-type brown dwarf companion or a dusty debris disc.

by 3800K, however, this does not significantly affect the result. This is a good example of where reddening is probably reducing the blue flux. Reddening the white dwarf model spectrum by $E(B - V) \simeq 0.05$ brings the overall SED in line with the SDSS optical spectrum. Modelling of the companion object proved inconclusive as to its spectral type (Table 7). SDSS J1557+0916 is a good candidate for having a dusty disc or low-mass companion based on its IR spectral shape.

6.2.5 SDSS J2220-0041

PHL 5038 (= SDSS J2220-0041) is a wide ($0.94''$) binary containing a cool ($\sim 8000\text{K}$) white dwarf with an $\sim \text{L8}$ companion, only the fourth white dwarf plus brown dwarf binary known (Steele et al. 2009).

6.3 Example Photometric IR Excess Candidates

As described in Sect. 5.1.2, we fitted *all* photometric objects satisfying our DA white dwarf constraint set (Table 1) with DA model spectra, independent on whether they also have an SDSS spectrum.

6.3.1 DA white dwarf candidates

6.3.1.1 SDSS J0959-0200 SDSS J0959-0200 is a photometric-only DA candidate with $T_{\text{eff}} = 12000^{+1160}_{-500}\text{K}$ and $\log(g) = 8.00^{+1.20}_{-0.22}$. The UKIDSS K -band magnitude shows a large (5σ) excess over the white dwarf model, no excess is seen at shorter wavelengths. This object is a strong candidate for having a very late type brown dwarf companion, or a dusty debris disc.

6.3.1.2 SDSS J1221+1245 A second interesting photometric-only DA white dwarf candidate is SDSS J1221+1245. The white dwarf is best fitted by a model with system parameters $T_{\text{eff}} = 12000^{+1110}_{-270}\text{K}$ and

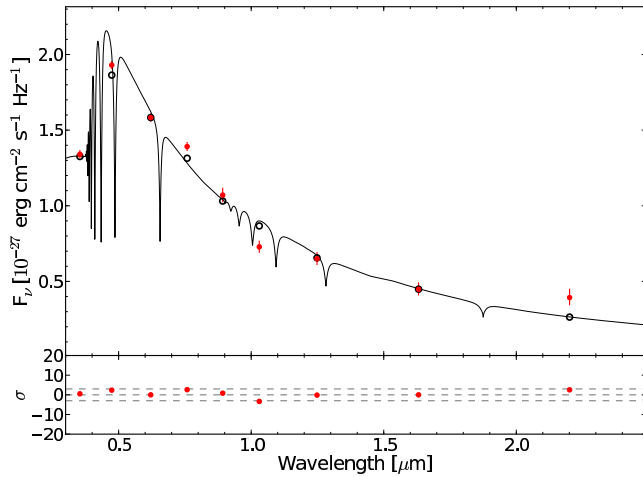


Figure 20. SDSS J1221+1245, a photometric-only DA white dwarf candidate ($T_{\text{eff}} = 12000 \pm_{270}^{1110}$ K, $\log(g) = 8.00 \pm_{0.34}^{0.51}$) that exhibits a borderline *K*-band excess. It is good candidate for having either a late-type brown dwarf companion or a dusty debris disc.

$\log(g) = 8.00 \pm_{0.34}^{0.51}$. The UKIDSS *K*-band magnitude shows a borderline excess over the white dwarf model, but no excess is seen at shorter wavelengths. This object is again a good candidate for having a very late type brown dwarf companion, or a dusty debris disc.

6.3.2 Other Composite Objects

Inspection of Simbad reveals that four of the photometric-only DA candidates with IR excess (DA:ire and DA:ire:, Table 8) are previously known (pre-)white dwarf binaries and one pulsating subdwarf, which provides a preview on the mixture of objects that can be expected within this sample. It also underlines that the method efficiently identifies genuine infrared-excess white dwarfs.

6.3.2.1 SDSS J0016+0704 = PG 0014+067

Brassard et al. (2001) identified PG 0014+067 as a pulsating sdB with $T_{\text{eff}} = 33550 \pm 380$ K and $\log(g) = 5.77 \pm 0.10$. Fitting the *ugri* photometry with DA model atmospheres results in $T_{\text{eff}} = 24000 \pm_{600}^{2100}$ K with the surface gravity fixed to $\log(g) = 8$, and reveals a clear IR excess. At such high temperatures, the slope of the optical and near-IR SED of this object is close to a Rayleigh-Jeans distribution, and while modelling the photometric data with DA models may not be perfect, we believe that PG 0014+067 does exhibit a genuine IR excess. In their asteroseismological analysis, Brassard et al. (2001) found that the pulsation frequency spectrum of PG 0014+067 exhibits fine structure that they tentatively interpreted as a rotational period of 29.2 ± 0.9 h, revised later by (Jeffery et al. 2005) to ~ 4 d. One possibility is that PG 0014+067 has a close low-mass binary companion with an orbital period of a few days and that the sdB is tidally locked, rotating at the same period. This hypothesis can be tested by a radial velocity study of this subdwarf.

6.3.2.2 Cataclysmic Variables

(= SDSS J0920+3356)

and

BK Lyn
HS 0139+0559

(= SDSS0141+0614) are novalike variables (Dobrzycka & Howell 1992; Aungwerojwit et al. 2005) with optically thick accretion discs, and their optical colours are similar to that of hot white dwarfs or subdwarfs. However, their companion stars and cooler outer regions of the accretion discs start to contribute noticeably in the near-IR.

6.3.2.3 Detached Binaries

Abell 31 (= SDSS J0854+0853, PN G219.1+31.2) is a planetary nebula with a nearby (0.26'') M-dwarf, both stars are most likely an associated wide binary (Ciardullo et al. 1999).

GK Vir (= SDSS J1415+0117) is an eclipsing binary containing a hot ($\simeq 48800$ K) white dwarf plus an $\sim M4V$ companion with an orbital period of 0.344 d (Green et al. 1978; Fulbright et al. 1993; Parsons et al. 2010).

7 COMPARISON WITH SDSS DR6 WHITE DWARF-MAIN SEQUENCE BINARIES

Rebassa-Mansergas et al. (2010, hereafter RM10) compiled a catalogue of white dwarf-main sequence (WDMS) binaries from all spectroscopic objects within SDSS DR6. Given that their detection method was based on optical data alone, RM10 were primarily sensitive to white dwarfs with M-type companions. The distribution of their WDMS binaries as a function of effective temperature and companion star spectral type shows a clear concentration of $T_{\text{eff}} = 10 - 20$ kK white dwarfs with $\sim M4$ -type companions (Fig. 21, left panel). The large luminosity of hot white dwarfs prevents the identification of low-mass companions around them, explaining the relative dearth of late spectral types at higher temperatures. The decreasing number of very late M-dwarfs ($> M6$) could also be affected to some degree by the same contrast problem, however, it is known that the companion mass distribution of WDMS binaries is dropping towards the low-mass end of the main sequence (Farihi et al. 2005).

The sample of WDMS binaries of RM10 provides a natural comparison for the work done here. We have subjected their entire sample of WDMS binaries to our DA colour cuts (Table 1), finding that only 93 of the 1602 systems fall within the colour cuts. This small number is not too surprising, as the red flux from the M-dwarf companions moves the majority of RM10's WDMS binaries out of our colour selection. RM10 list WD temperature *and* companion spectral type for 53 of these 93 systems. In contrast to our work here (Sect. 5.2), the study of RM10 included (partially) resolved systems. Consequently, we removed 21 that appeared resolved in the SDSS (or UKIDSS images where available), which leaves us with 32 objects in common. Figure 21 shows that the two samples only overlap for systems where the companion is relatively faint in the optical compared to the white dwarf, which is expected as our DA selection needs the white dwarf to dominate. Finally, 10 of the 32 objects are in the UKIDSS footprint.

We cross-correlated the white dwarfs with an IR excess from our spectroscopic and photometric samples (Table 7 and 8), and the WDMS catalogue of RM10 and found 19 objects in common (Table 10). This is comprised of the 10 objects above that we expect to be in the sample, along

with 9 others where no spectral type is listed in RM10's catalogue. There is in general a good agreement between the white dwarf system parameters, however the underestimation of photometric temperatures is highlighted again. The spectroscopic sample and the WDMS catalogue largely find companion types within two spectral types of each other. All of these are M-type companions as expected from the sensitivity of the WDMS catalogue. Five objects are found to have an excess in the photometric method, but were rejected from the spectroscopic sample because signatures of a main sequence star companion can be seen in the optical spectra, whereas the spectroscopic sample only contains pure DA white dwarfs. Those are marked as such in Table 10, and suffer from the same companion type biases discussed in Section 5.4.1.

8 CONFIRMATION OF IR EXCESS CANDIDATES IN WISE

We cross correlated all spectroscopic and photometric-only IR excess candidates (from Table 7 and 8 respectively) with WISE PDR within $2.5''$. Of the 42 IR excess objects from the spectroscopic method, 3 had a detection in at least one WISE band. Similarly 14 of the 67 photometric-only objects were detected and are listed in the online master table.

The three spectroscopically confirmed DA white dwarfs with IR excesses and WISE data: SDSS J0236–0103, SDSS J0847+2831 and SDSS J1448+0713, are all confirmed to have an excess in the WISE 3.4 and $4.6\mu\text{m}$ bands. They are however all predicted to have late M-type companions and are not brown dwarf or debris disk candidates.

Of the 14 photometric-only IR excess candidates with WISE data, SDSS J1524–0128 and SDSS J1549+0325 are *not* found to have an excess in the 3.4 and $4.6\mu\text{m}$ bands. Similarly, because we do not trust the effective temperature of the white dwarf fit, we also do not believe the far-IR excess found for SDSS J0841+0501, SDSS J1441+0137, SDSS J1538+0644 and SDSS J1551–0118. This is indicated by a flat, constant excess over the white dwarf model and is continued into the far-IR WISE data in these cases (see Fig. 22).

The remaining 8 objects (SDSS J0207+0715, SDSS J0742+2857, SDSS J0751+2002, SDSS J0920+3356, SDSS J1448+0812, SDSS J1456+1040, SDSS J1538+2957, and SDSS J1635+2912) are confirmed to have an IR excess consistent with a late type companion in the WISE far-IR data. Some interesting examples of these are shown in Fig. 23. SDSS J1538+2957 (Fig. 23) is predicted to have an M8-type companion from the photometric method. However, the spectral shape of the excess is found to be inconsistent with such an early type companion. The excess in UKIDSS, and now WISE, is more indicative of a later type brown dwarf companion or dusty debris disk. This mismatch is most likely caused by over estimating the distance to the white dwarf in the photometric method. SDSS J1635+2912 (Fig. 23) is one of the photometric-only debris disk candidate systems. The WISE $3.5\mu\text{m}$ flux confirms the infrared excess, but still leaves the origin of the excess, brown dwarf or disk, open.

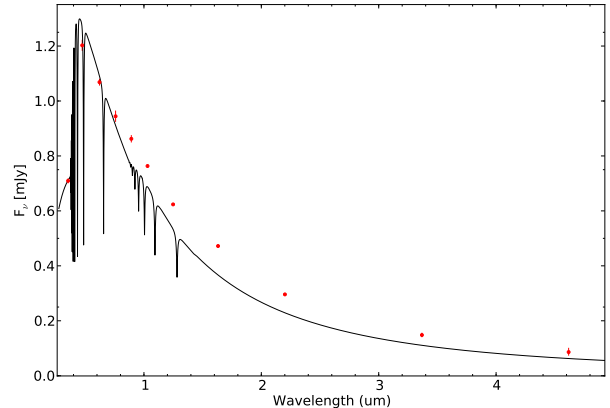


Figure 22. SED of SDSS J1538+0644. The SDSS, UKIDSS and WISE 3.4 and $4.6\mu\text{m}$ fluxes are shown as red circles. The best fit white dwarf model to the SDSS photometry is shown as a black line. The shape of the IR excess is not consistent with any companion or disk. It is more likely that the excess is an artifact of overestimating the white dwarf effective temperature.

9 DISCUSSION

9.1 Selection of DA white dwarfs from optical photometry

We have developed dedicated colour-colour cuts to select DA white dwarfs only from their optical photometry (Table 1, Fig. 2). This method can easily be optimised to prioritise for completeness, efficiency or a compromise of both. We have demonstrated that a high completeness (95.4%) can be obtained with a reasonable efficiency (62.3%) based on the *ugriz* data from SDSS DR7. The strengths of this approach, is that it provides substantially larger and statistically better characterised white dwarf samples (Sect. 3.3) when compared to spectroscopic catalogues such as McCook & Sion (1999) and Eisenstein et al. (2006). We have also investigated methods to account for the contamination of the DA white dwarf candidate sample by quasars and NLHS. This method can be adapted to obtain large uniform samples of white dwarfs from other multicolour optical photometric surveys, such as e.g. SkyMapper (Keller et al. 2007).

9.2 Implications for the brown dwarf desert and the numbers of white dwarfs with dusty debris discs

Fitting the optical spectroscopy or photometry and probing for IR flux excess above the best-fit white dwarf, as previously done by Tremblay & Bergeron (2007), has proven to be an efficient and robust approach. It also allows one to identify hot white dwarfs with low-level excesses which have IR colours that are very similar to the bulk population of white dwarfs (Fig. 13). Our search is sensitive to companions as late as $\sim\text{L8}$, and to warm dusty debris discs.

Of the 1275 spectroscopically confirmed DA white dwarfs with at least one UKIDSS magnitude, 26 (2.0%) are found (or are candidates) to have an IR excess consistent with a L0-type companion or later, i.e. a brown dwarf. The exact cut off of where the brown dwarf sequence starts is age dependent and can vary from mid-M to mid-L-type. Taking

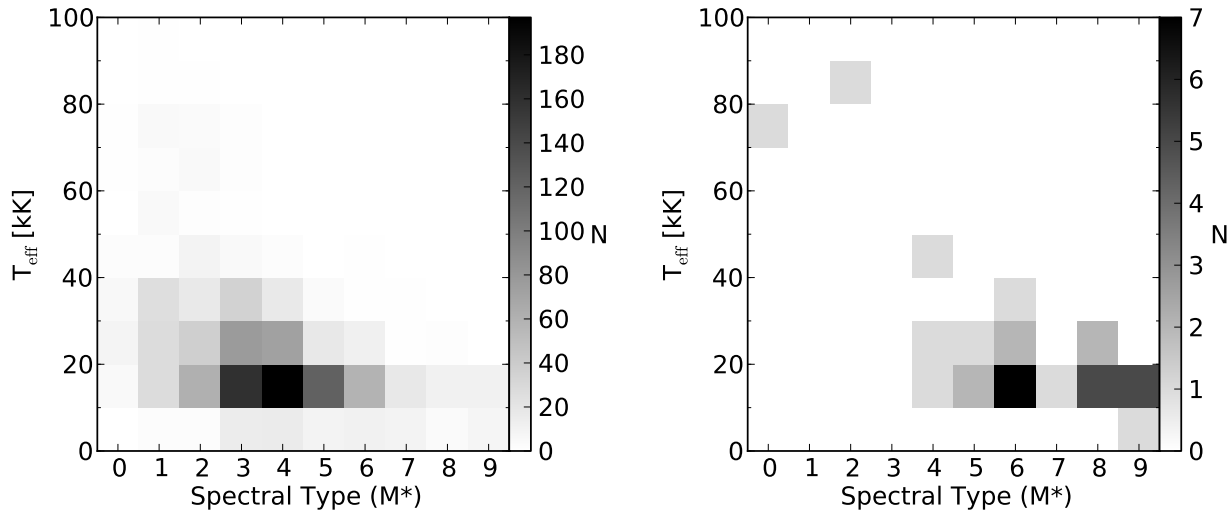


Figure 21. The distribution of the WDMS binaries from the catalogue of Rebassa-Mansergas et al. (2010) as a function of effective temperature of the white dwarf and spectral type of the companion star. The left hand panel shows all the 1173 objects with values for both T_{eff} and $\log(g)$. 53 of these are contained within the colour-colour region defined in Table 1. Excluding spatially resolved binaries leaves 32 objects satisfying all the criteria of our DA white dwarf selection, which are shown in the right hand panel.

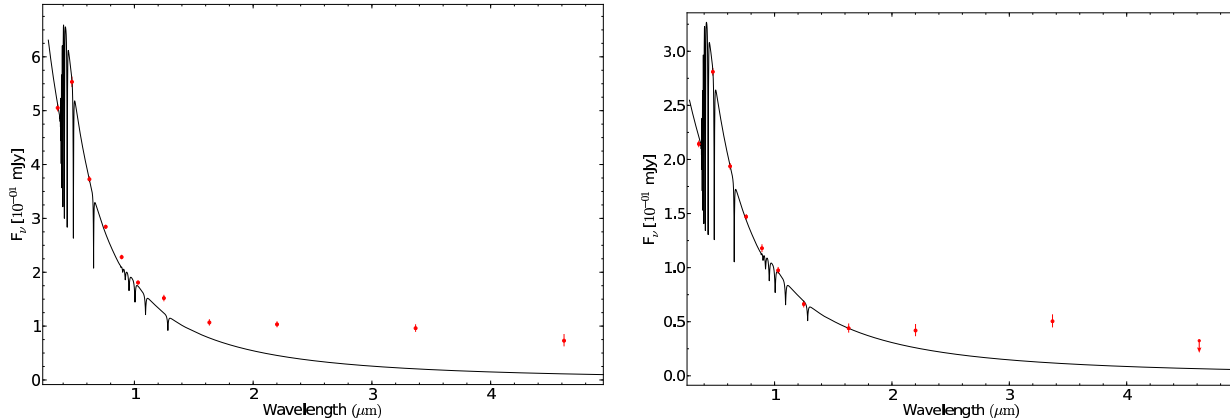


Figure 23. SEDs of SDSS J1538+2957 (left) and SDSS J1635+2912 (right). The plot follows the same format as Fig. 22. SDSS J1538+2957 and SDSS J1635+2912 are predicted herein to have an M7: and an L6:-type companion or potential debris disk respectively.

the white dwarf mass distribution and the initial-final mass relation we can calculate the white dwarf progenitor masses. This with the white dwarf cooling age allows us to estimate the total age of the system. The average total age of the companion is a few Gyr, and in this regime L0-type is a suitable cut-off for being a brown dwarf. Taking only the systems where we are confident of the excess (not “DAire:” in Table 7) gives a lower limit for the number of white dwarfs with brown dwarf type companions of 0.8%. This is compatible with previous estimates. An adaptive optics imaging survey of 266 solar-like stars by Metchev & Hillenbrand (2009) found a wide (28–1590 AU) sub-stellar companion fraction of $3.2^{+3.1}_{-2.7}\%$. Farihi et al. (2005) carried out an extensive near-IR imaging survey for both wide and unresolved low-mass companions to 394 known white dwarfs, finding an overall stellar companion fraction of 22%, and a brown dwarf companion fraction of $< 0.5\%$.

When using the photometric fitting method, 105 of the 1771 photometric-only DA white dwarf candidates with UKIDSS data exhibit an IR excess, of which we eliminate 38

likely quasars (Sect. 5.4.2 and see online QSO table). Taking into account our estimate for the contamination by NLHS (Sect. 5.4.3), we find that $\sim 2.7\%$ of white dwarfs in the photometric-only sample have an IR excess, of which 1.8% are candidates for having a brown dwarf companion. This is consistent with the frequencies found in the spectroscopic sample, though not as secure.

Taking only the objects with a detection in the K -band (required for detecting a disk), of the 571 spectroscopically confirmed DA white dwarfs, 7 (1.2%) are found to have an IR excess compatible with a companion spectral type later or equal to L8, and are hence viable disc candidates. Similarly, 0.5% (4/840) of the photometric-only sample are disc candidates, or, scaling for the 62.3% efficiency of our DA white dwarf selection, 0.8% (4/523). This is consistent with the results of Farihi et al. (2009), who estimated that the frequency of white dwarfs with dusty debris discs is at least 1%. Any search for debris discs based on K -band data is biased towards warm, bright circumstellar dust rather than faint discs or narrow rings. Of the known white dwarfs with

a dusty debris disc, only about half reveal themselves shortward of $3\mu\text{m}$ (Kilic et al. 2006; Farihi et al. 2009).

To confirm the IR excess candidates we have cross matched all the spectroscopic (Table 7) and photometric-only (Table 8) candidates with the far-IR WISE PDR. This has provided 3.4 and $4.6\mu\text{m}$ fluxes for 7% (3/42) and 21% (14/64) of the spectroscopic and photometric-only IR excess candidates respectively. We find that all three of the spectroscopic IR excess candidates also have an excess in the far-IR.

However, in the photometric-only sample, a total of six objects are found not to have a definite IR excess at $> 3\mu\text{m}$. The remaining 8 of 14 white dwarf candidates have a real IR excess in the WISE fluxes. We therefore find that $\sim 60\%$ of the photometric-only IR excess candidates have real IR excesses consistent with a MS star companion, brown dwarf companion or dusty debris disk.

Determining the true nature of the white dwarfs with an excess in K only will require far-IR data to distinguish between a late-type brown dwarf companion or a dusty debris disc. More generally, deeper near-IR and/or far-IR follow up observations will be required to verify, or refute, the IR excess candidates (DAire: and DA:ire:), as some of these candidates are likely to be spurious. Similarly, while our colour selection (Table 1) has a high efficiency, optical spectroscopy of the white dwarf candidates (DA:ire and DA:ire:) will be necessary to confirm their (DA) white dwarf nature.

10 CONCLUSIONS

We have developed a detailed method to select DA white dwarfs in *ugriz* colour space, and applying this method to SDSS DR7, we have identified 7444 DA white dwarfs with $g \leq 19$ and SDSS spectroscopy, approximately 70% more than the corresponding number from DR4 (Eisenstein et al. 2006), and 9341 photometric-only DA candidates. Using this sample, we estimate the spectroscopic completeness of DA white dwarfs with $T \gtrsim 8000\text{ K}$ in SDSS DR7 to be $\simeq 44\%$.

We cross-correlated these spectroscopic and photometric DA samples with UKIDSS DR8 to carry out the currently largest and deepest untargeted search for low-mass companions to and debris discs around DA white dwarfs. This search led to the identification of a significant number of DA white dwarfs with low-mass companions, including several brown dwarf and dusty debris disc candidates. Similar studies to the one presented here making use of the full UKIDSS area, as well as the corresponding surveys in the southern hemisphere, e.g. Skymapper, VISTA and VHS, promise to further increase the sample sizes of these types of systems.

NOTE

Before submission the authors became aware of the study of Steele et al. (2011, in prep.) who have carried out an independent study, cross-matching the spectroscopically confirmed white dwarfs from McCook & Sion (1999) and Eisenstein et al. (2006) with UKIDSS DR8. Comparison of their results with our spectroscopic sample shows that both studies lead to broadly consistent results.

ACKNOWLEDGEMENTS

Funding for the Sloan Digital Sky Survey (SDSS) and SDSS-II has been provided by the Alfred P. Sloan Foundation, the Participating Institutions, the National Science Foundation, the U.S. Department of Energy, the National Aeronautics and Space Administration, the Japanese Monbukagakusho, and the Max Planck Society, and the Higher Education Funding Council for England. The SDSS Web site is <http://www.sdss.org/>.

D. Steeghs acknowledges a STFC Advanced Fellowship.

This publication makes use of data products from the Wide-field Infrared Survey Explorer, which is a joint project of the University of California, Los Angeles, and the Jet Propulsion Laboratory/California Institute of Technology, funded by the National Aeronautics and Space Administration.

REFERENCES

- Aannestad, P. A., Kenyon, S. J., Hammond, G. L., Sion, E. M., 1993, *AJ*, 105, 1033
- Abazajian, K. N., et al., 2009, *ApJS*, 182, 543
- Araujo-Betancor, S., Gänsicke, B. T., Long, K. S., Beuermann, K., de Martino, D., Sion, E. M., Szkody, P., 2005, *ApJ*, 622, 589
- Aungwerojwit, A., et al., 2005, *A&A*, 443, 995
- Becklin, E. E., Zuckerman, B., 1988, *Nat*, 336, 656
- Bergeron, P., Saffer, R. A., Liebert, J., 1992, *ApJ*, 394, 228
- Beuermann, K., Wheatley, P., Ramsay, G., Euchner, F., Gänsicke, B. T., 2000, *A&A*, 354, L49
- Brassard, P., Fontaine, G., Billères, M., Charpinet, S., Liebert, J., Saffer, R. A., 2001, *ApJ*, 563, 1013
- Brinkworth, C. S., Gänsicke, B. T., Marsh, T. R., Hoard, D. W., Tappert, C., 2009, *ApJ*, 696, 1402
- Burleigh, M. R., Clarke, F. J., Hodgkin, S. T., 2002, *MNRAS*, 331, L41
- Burleigh, M. R., et al., 2006, *MNRAS*, 373, 1416
- Burleigh, M. R., et al., 2008, *MNRAS*, 386, L5
- Ciardullo, R., Bond, H. E., Sipior, M. S., Fullton, L. K., Zhang, C., Schaefer, K. G., 1999, *AJ*, 118, 488
- Covey, K. R., et al., 2007, *AJ*, 134, 2398
- De Gennaro, S., von Hippel, T., Winget, D. E., Kepler, S. O., Nitta, A., Koester, D., Althaus, L., 2008, *AJ*, 135, 1
- Debes, J. H., López-Morales, M., Bonanos, A. Z., Weinberger, A. J., 2006, *ApJ Lett.*, 647, L147
- Dobrzycka, D., Howell, S. B., 1992, *ApJ*, 388, 614
- Dupuis, J., Fontaine, G., Pelletier, C., Wesemael, F., 1993, *ApJS*, 84, 73
- Dye, S., et al., 2006, *MNRAS*, 372, 1227
- Eisenstein, D. J., et al., 2006, *ApJS*, 167, 40
- Farihi, J., Christopher, M., 2004, *AJ*, 128, 1868
- Farihi, J., Becklin, E. E., Zuckerman, B., 2005, *ApJS*, 161, 394
- Farihi, J., Burleigh, M. R., Hoard, D. W., 2008, *ApJ*, 674, 421
- Farihi, J., Jura, M., Zuckerman, B., 2009, *ApJ*, 694, 805
- Farihi, J., Barstow, M. A., Redfield, S., Dufour, P., Hambly, N. C., 2010, *MNRAS*, 404, 2123
- Fulbright, M. S., Liebert, J., Bergeron, P., Green, R., 1993, *ApJ*, 406, 240

- Gänsicke, B. T., Beuermann, K., de Martino, D., 1995, *A&A*, 303, 127
- Gänsicke, B. T., Long, K. S., Barstow, M. A., Hubeny, I., 2006a, *ApJ*, 639, 1039
- Gänsicke, B. T., Marsh, T. R., Southworth, J., Rebassa-Mansergas, A., 2006b, *Science*, 314, 1908
- Gänsicke, B. T., Marsh, T. R., Southworth, J., 2007, *MNRAS*, 380, L35
- Graham, J. R., Matthews, K., Neugebauer, G., Soifer, B. T., 1990, *ApJ*, 357, 216
- Green, R. F., Richstone, D. O., Schmidt, M., 1978, *ApJ*, 224, 892
- Grether, D., Lineweaver, C. H., 2006, *ApJ*, 640, 1051
- Han, Z., Podsiadlowski, P., Maxted, P. F. L., Marsh, T. R., 2003, *MNRAS*, 341, 669
- Heber, U., 2009, *ARA&A*, 47, 211
- Hoard, D. W., Wachter, S., Sturch, L. K., Widhalm, A. M., Weiler, K. P., Pretorius, M. L., Wellhouse, J. W., Gibiansky, M., 2007, *AJ*, 134, 26
- Hogan, E., Burleigh, M. R., Clarke, F. J., 2009, *MNRAS*, 396, 2074
- Holberg, J. B., Bergeron, P., 2006, 132, 1221
- Holberg, J. B., Bergeron, P., Gianninas, A., 2008, *AJ*, 135, 1239
- Howell, S. B., Harrison, T. E., Huber, M. E., Szkody, P., Walter, F. M., Harbeck, D., 2008, *AJ*, 136, 2541
- Ignace, R., 2001, *PASP*, 113, 1227
- Jeffery, C. S., Aerts, C., Dhillon, V. S., Marsh, T. R., Gänsicke, B. T., 2005, *MNRAS*, 362, 66
- Jura, M., 2003, *ApJ Lett.*, 584, L91
- Keller, S. C., et al., 2007, *Publications of the Astronomical Society of Australia*, 24, 1
- Kilic, M., von Hippel, T., Leggett, S. K., Winget, D. E., 2006, *ApJ*, 646, 474
- Kilic, M., Brown, W. R., Allende Prieto, C., Pinsonneault, M. H., Kenyon, S. J., 2007, *ApJ*, 664, 1088
- Koester, D., 2010, *Memorie della Societa Astronomica Italiana*, 81, 921
- Koester, D., Wilken, D., 2006, *A&A*, 453, 1051
- Koester, D., Schulz, H., Weidemann, V., 1979, *A&A*, 76, 262
- Koester, D., Provencal, J., Shipman, H. L., 1997, *A&A*, 320, L57
- Lawrence, A., et al., 2007, *MNRAS*, 379, 1599
- Li, N., Thakar, A. R., 2008, *Computing in Science and Engineering*, 10, 18
- Liebert, J., Bergeron, P., Eisenstein, D., Harris, H. C., Kleinman, S. J., Nitta, A., Krzesinski, J., 2004, *ApJ Lett.*, 606, L147
- Liebert, J., Bergeron, P., Holberg, J. B., 2005, *ApJS*, 156, 47
- Linnell, A. P., Szkody, P., Plotkin, R. M., Holtzman, J., Seibert, M., Harrison, T. E., Howell, S. B., 2010, *ApJ*, 713, 1183
- Luhman, K. L., Burgasser, A. J., Bochanski, J. J., 2011, *ApJ Lett.*, 730, L9+
- Marcy, G. W., Butler, R. P., 2000, *PASP*, 112, 137
- Marsh, T., Gänsicke, B. T., Steeghs, D., Southworth, J., Koester, D., Harris, V., Merry, L., 2010, *ApJ Lett.*, submitted, arXiv:1002.4677
- Maxted, P. F. L., Napiwotzki, R., Dobbie, P. D., Burleigh, M. R., 2006, *Nat*, 442, 543
- McCook, G. P., Sion, E. M., 1999, *ApJS*, 121, 1
- Melis, C., Jura, M., Albert, L., Klein, B., Zuckerman, B., 2010, *ApJ*, 722, 1078
- Metchev, S. A., Hillenbrand, L. A., 2009, *ApJS*, 181, 62
- Mullally, F., Reach, W. T., Degennaro, S., Burrows, A., 2009, *ApJ*, 694, 327
- Oswalt, T. D., Smith, J. A., Wood, M. A., Hintzen, P., 1996, *Nat*, 382, 692
- Parsons, S. G., et al., 2010, *MNRAS*, 407, 2362
- Probst, R. G., Oconnell, R. W., 1982, *ApJ Lett.*, 252, L69
- Rebassa-Mansergas, A., Gänsicke, B. T., Rodríguez-Gil, P., Schreiber, M. R., Koester, D., 2007, *MNRAS*, 382, 1377
- Rebassa-Mansergas, A., Gänsicke, B. T., Schreiber, M. R., Koester, D., Rodríguez-Gil, P., 2010, *MNRAS*, 402, 620
- Schlegel, D. J., Finkbeiner, D. P., Davis, M., 1998, *ApJ*, 500, 525
- Schmidt, G. D., Szkody, P., Silvestri, N. M., Cushing, M. C., Liebert, J., Smith, P. S., 2005, *ApJ Lett.*, 630, L173
- Schmidt, G. D., et al., 2003, *ApJ*, 595, 1101
- Steele, P. R., Burleigh, M. R., Farihi, J., Gänsicke, B. T., Jameson, R. F., Dobbie, P. D., Barstow, M. A., 2009, *A&A*, 500, 1207
- Stoughton, C., et al., 2002, *AJ*, 123, 485
- Tremblay, P.-E., Bergeron, P., 2007, *ApJ*, 657, 1013
- Tremblay, P.-E., Bergeron, P., 2009, *ApJ*, 696, 1755
- Wachter, S., Hoard, D. W., Hansen, K. H., Wilcox, R. E., Taylor, H. M., Finkelstein, S. L., 2003, *ApJ*, 586, 1356
- Winget, D. E., Hansen, C. J., Liebert, J., van Horn, H. M., Fontaine, G., Nather, R. E., Kepler, S. O., Lamb, D. Q., 1987, *ApJ Lett.*, 315, L77
- Wright, E. L., et al., 2010, 140, 1868
- Yanny, B., et al., 2009, *AJ*, 137, 4377
- York, D. G., et al., 2000, *AJ*, 120, 1579
- Zuckerman, B., Becklin, E. E., 1987, *Nat*, 330, 138

This paper has been typeset from a \LaTeX file prepared by the author.

Table 7. 42 DA white dwarf IR excess candidates from the spectroscopic method. In all columns, ‘?’ indicates an uncertain classification. The notes column indicates the level of certainty of the IR excess. The key to the notes2 column is: bg (background contamination), disc (disc candidate), moreIR (more IR data required), resolved (resolved or partially resolved binary). The “Eisenstein” column is the classifications according to the Eisenstein et al. (2006) catalogue. The column “JHK” firstly indicates whether the object has a UKIDSS J , H and/or K magnitude. Secondly, if the corresponding letter is bold, it means an excess was found in that band.

Coord	$T_{\text{eff}}(K)$	$\log(g)$	$M_{\text{wd}}(M_{\odot})$	$R_{\text{wd}}(10^8 \text{ cm})$	$d(pc)$	Companion	Notes	Notes2	Eisenstein	JHK
0032+0739	21045 ± 249	7.42 ± 0.05	0.37 ± 0.02	1.37 ± 0.05	398 ± 15	M6	DAire:	resolved,bg:	DA	JHK
0039–0030	12392 ± 544	7.35 ± 0.16	0.32 ± 0.05	1.37 ± 0.15	417 ± 44	M9	DAire:		DA_auto	JHK
0135+1445	7467 ± 18	7.34 ± 0.04	0.29 ± 0.01	1.33 ± 0.03	69 ± 2	L6	DAire		DA	JHK
0207+0702	10073 ± 77	8.32 ± 0.09	0.80 ± 0.06	0.72 ± 0.05	162 ± 10	L7	DAire:			JHK
0236–0103	20566 ± 498	7.66 ± 0.09	0.46 ± 0.04	1.15 ± 0.07	411 ± 25	M6	DAire		DA+M:	JHK
0253–0027	18974 ± 286	7.71 ± 0.06	0.47 ± 0.03	1.11 ± 0.05	380 ± 15	L4	DAire	moreIR	DA_auto	JH
0748+2058	86726 ± 7732	7.15 ± 0.27	0.53 ± 0.06	2.23 ± 1.37	2021 ± 469	M3	DAire	resolved:	DA+M:	JHK
0753+2447	13432 ± 710	7.81 ± 0.15	0.50 ± 0.08	1.02 ± 0.10	349 ± 32	L5:	DAire	disk	DA_auto	JHK
0847+2831	12828 ± 930	7.76 ± 0.20	0.48 ± 0.11	1.05 ± 0.14	357 ± 42	M6	DAire		DA+M:	JHK
0907+0536	19416 ± 458	7.78 ± 0.09	0.51 ± 0.05	1.06 ± 0.06	367 ± 21	L6	DAire:	moreIR	DA_auto	JHK
0933+3200	11565 ± 381	8.36 ± 0.20	0.83 ± 0.13	0.70 ± 0.11	229 ± 34	L4	DAire	resolved:		JHK
0950+0115	21785 ± 365	7.89 ± 0.06	0.57 ± 0.03	0.99 ± 0.04	329 ± 14	L8	DAire:	moreIR	DA	JH
1002+0939	21785 ± 808	7.92 ± 0.14	0.58 ± 0.08	0.97 ± 0.09	515 ± 45	L0	DAire		DA_auto	JHK
1010+0407	13588 ± 668	7.76 ± 0.11	0.48 ± 0.05	1.05 ± 0.07	280 ± 18	L8:	DAire:	moreIR	DA_auto	JH
1015+0425	34526 ± 86	7.38 ± 0.07	0.41 ± 0.02	1.51 ± 0.08	691 ± 39	L4	DAire:	moreIR	DA_auto	JHK
1016+0020	21045 ± 703	8.48 ± 0.12	0.92 ± 0.07	0.64 ± 0.06	325 ± 32	L6	DAire:	moreIR	DA	H
1037+0139	11433 ± 208	8.38 ± 0.13	0.84 ± 0.08	0.69 ± 0.07	151 ± 14	L5:	DAire		DA	JHK
1120+0639	20331 ± 609	7.69 ± 0.11	0.47 ± 0.05	1.13 ± 0.09	517 ± 38	L3	DAire:	resolved,bg:	DA_auto	J
1141+0420	11835 ± 818	7.37 ± 0.22	0.32 ± 0.08	1.35 ± 0.21	317 ± 46	M7	DAire		DA+M:	JHK
1208+0610	23076 ± 1125	7.64 ± 0.17	0.46 ± 0.08	1.18 ± 0.14	725 ± 81	M7	DAire		DA_auto	JH
1218+0042	11173 ± 180	8.30 ± 0.11	0.79 ± 0.07	0.73 ± 0.06	171 ± 13	L8	DAire:	moreIR	DA	JH
1228+1040	22037 ± 199	8.19 ± 0.04	0.74 ± 0.02	0.80 ± 0.02	134 ± 3	L6:	DAire	disk	DA_auto	JHK
1246+0707	10793 ± 189	8.03 ± 0.16	0.62 ± 0.10	0.88 ± 0.10	200 ± 21	L2	DAire			HK
1247+1035	17912 ± 159	7.82 ± 0.04	0.52 ± 0.02	1.03 ± 0.03	394 ± 9	L6:	DAire:	bg:,resolved:		JHK
1314+0057	17707 ± 163	7.80 ± 0.04	0.51 ± 0.02	1.04 ± 0.03	312 ± 8	L6	DAire:	disk:		HK
1320+0018	19193 ± 213	8.40 ± 0.04	0.87 ± 0.03	0.68 ± 0.02	142 ± 5	L8	DAire:	disk:	DA	JHK
1329+1230	13432 ± 272	7.42 ± 0.05	0.34 ± 0.02	1.32 ± 0.05	209 ± 8	M7	DAire		DA_auto	JHK
1331+0040	15964 ± 714	7.72 ± 0.17	0.47 ± 0.08	1.09 ± 0.12	465 ± 48	?	DAire:	moreIR	DA	
1341+0056	18330 ± 436	7.99 ± 0.10	0.61 ± 0.06	0.92 ± 0.06	360 ± 22	M7	DAire			JHK
1352+0910	36154 ± 722	7.49 ± 0.11	0.45 ± 0.04	1.39 ± 0.13	849 ± 76	M5	DAire			JHK
1410+0225	11565 ± 246	8.63 ± 0.13	1.00 ± 0.07	0.56 ± 0.06	152 ± 16	$\geq L8$	DAire:	moreIR	DA	JH
1425–0013	10670 ± 169	7.97 ± 0.17	0.58 ± 0.10	0.91 ± 0.10	242 ± 26	L8:	DAire:	moreIR	DA	JHK
1448+0240	14728 ± 247	7.41 ± 0.06	0.34 ± 0.02	1.34 ± 0.06	292 ± 13	L4	DAire	moreIR	DA	JH
1448+0713	12250 ± 256	7.87 ± 0.09	0.53 ± 0.05	0.98 ± 0.06	143 ± 8	M8	DAire			JHK
1450+0000	17106 ± 175	7.93 ± 0.05	0.58 ± 0.03	0.95 ± 0.03	311 ± 9	L8:	DAire:	moreIR		JHK
1557+0916	22811 ± 734	7.75 ± 0.11	0.50 ± 0.05	1.09 ± 0.08	488 ± 35	L1:	DAire		DA_auto	JHK
1609+2905	8773 ± 91	8.26 ± 0.14	0.76 ± 0.09	0.75 ± 0.08	122 ± 12	$\geq L8$	DAire			JHK
1619+2533	25595 ± 1139	7.21 ± 0.15	0.33 ± 0.04	1.65 ± 0.20	879 ± 101	M5	DAire			JHK
1625+3026	72136 ± 4550	7.77 ± 0.19	0.64 ± 0.08	1.21 ± 0.21	739 ± 112	M5	DAire		DA_auto	JHK
2220–0041	7467 ± 21	7.66 ± 0.12	0.41 ± 0.06	1.10 ± 0.08	69 ± 5	$\geq L8$	DAire:	resolved	DA_auto	JHK
2225+0016	11045 ± 235	8.44 ± 0.16	0.88 ± 0.10	0.65 ± 0.08	167 ± 20	L6	DAire:	resolved:	DA_auto	JHK
2331+1342	11173 ± 284	8.79 ± 0.15	1.09 ± 0.08	0.49 ± 0.07	141 ± 19	L6	DAire		DA+M:	JHK

Table 8. 67 photometric-only IR excess candidates which are found to have an IR excess in the photometric method. The columns follow the same format as that in Table 7. The key to the "Notes2" column is: bf (visually bad fit), bg (background contamination), disc (disc candidate), hotWD (high T_{eff} white dwarf and so small changes in, e.g. flux calibration, remove the excess), moreIR (more IR data required), resolved (resolved or partially resolved binary), qso (quasar), ? (unknown). Also, the "Simbad Name" and "Simbad Class" columns give an indication of what is already known about the objects. If the surface gravity could not be constrained, it was assigned the canonical value of 8.0 and therefore no error could be defined. We do not quote the distances to the systems because the uncertainty is so large. The two objects marked as "QSO:" are borderline cases of the objects found in the online QSO table and are therefore left as candidates for being DA white dwarfs with an IR excess.

Coord	$T_{\text{eff}}(K)$	$\log(g)$	Companion	Notes	Notes2	JHK	Simbad Name	Simbad Class
0016+0704	$24000 \pm^{2100}_{600}$	8.00	L0	DA:ire		JHK	V* EK Psc	Variable Star
0104+1459	$12000 \pm^{110}_{50}$	$7.75 \pm^{0.12}_{0.05}$	L5	DA:ire	moreIR	JH		
0141+0614	$11000 \pm^{70}_{1040}$	$8.50 \pm^{0.08}_{0.77}$	L8:	DA:ire:	bf	JHK	2MASS	Nova
0207+0715	$14000 \pm^{2140}_{1940}$	$9.25 \pm^{1.37}_{0.25}$	L6:	DA:ire	bf	JHK	PB6668	Star
0742+2857	$9000 \pm^{50}_{120}$	$7.25 \pm^{0.12}_{0.28}$	L6	DA:ire		JHK		
0751+2002	$20000 \pm^{2460}_{1140}$	$8.25 \pm^{3.25}_{1.25}$	L5	DA:ire		JHK		
0758+2406	$13000 \pm^{660}_{80}$	$8.00 \pm^{0.29}_{0.12}$	L2:	DA:ire		JHK		
0841+0501	$8000 \pm^{100}_{300}$	8.00	$\geq L8$:	DA:ire:	bf	JHK		
0842+0004	$22000 \pm^{100}_{220}$	8.00	M9	DA:ire		JH		
0854+0853	$60000 \pm^{6890}_{7210}$	8.00	M6	DA:ire		JHK	PN_A66_31	PN
0906+0001	$7000 \pm^{10}_{0}$	8.00	$\geq L8$:	DA:ire:	bf	JHK		
0920+3356	$12000 \pm^{90}_{110}$	$9.00 \pm^{0.28}_{0.15}$	L8:	DA:ire:	bf	JHK	V* BK Lyn	Nova
0923+0652	$7000 \pm^{10}_{0}$	8.00	$\geq L8$:	DA:ire:	bf,bg	JHK		
0925-0140	$14000 \pm^{80}_{140}$	$7.50 \pm^{0.28}_{0.37}$	M9	DA:ire		JHK		
0952+1205	$26000 \pm^{1540}_{2310}$	8.00	$\geq L8$:	DA:ire:	bf	HK		
0959-0200	$12000 \pm^{1160}_{500}$	$8.00 \pm^{1.20}_{0.22}$	L6	DA:ire	disk	JHK		
0959+0330	$32000 \pm^{2010}_{2570}$	8.00	L0	DA:ire		JHK	PG0957+037	UV
1005-0225	$14000 \pm^{50}_{120}$	$7.75 \pm^{0.45}_{0.13}$	L5:	DA:ire:	bf	JHK		
1006+0032	$20000 \pm^{470}_{830}$	$9.50 \pm^{0.91}_{0.17}$	L8	DA:ire	bf:	JHK	PG1004+008	UV
1038+1100	$10000 \pm^{170}_{90}$	$7.75 \pm^{0.17}_{0.27}$	L3	DA:ire		JHK		
1057+0628	$7000 \pm^{30}_{10}$	8.00	L8:	DA:ire:	QSO:	JHK		
1103+0101	$7000 \pm^{10}_{0}$	8.00	$\geq L8$:	DA:ire:	bf:	JHK	[VV2006]J110336.3+010141	Quasar
1103+1100	$34000 \pm^{260}_{2010}$	8.00	L4	DA:ire:	hotWD,moreIR	J	PG1101+113	SD
1116+0755	$22000 \pm^{2040}_{110}$	8.00	M9	DA:ire		JHK		
1153+0048	$15000 \pm^{1180}_{560}$	$9.50 \pm^{0.36}_{0.51}$	$\geq L8$:	DA:ire:	bf	JHK	LBQS1151+0104	Star
1221+1245	$12000 \pm^{1110}_{270}$	$8.00 \pm^{0.51}_{0.34}$	L8:	DA:ire:	disk:	JHK		
1224+0907	$7000 \pm^{30}_{30}$	8.00	L7	DA:ire:	bg:,resolved:,bf:	JHK		
1237-0151	$20000 \pm^{40}_{520}$	$8.75 \pm^{0.32}_{0.16}$	L4:	DA:ire:	resolved,bg:	JHK		
1246+1600	$19000 \pm^{610}_{530}$	$9.50 \pm^{0.40}_{0.16}$	$\geq L8$:	DA:ire:	bf:	JHK		
1315+0245	$28000 \pm^{1500}_{1790}$	8.00	L1:	DA:ire:	resolved,bg:	JHK		
1319+0152	$16000 \pm^{150}_{60}$	$8.25 \pm^{0.36}_{0.28}$	$\geq L8$:	DA:ire:	bf	HK	WD1317+021	DA
1323+2615	$17000 \pm^{1070}_{520}$	$9.50 \pm^{0.89}_{0.16}$	$\geq L8$:	DA:ire:	bf	HK		
1334+0534	$30000 \pm^{2410}_{390}$	8.00	$\geq L8$:	DA:ire:	bf:	HK		
1348+1100	$22000 \pm^{330}_{1180}$	8.00	L1	DA:ire	moreIR	J		
1355+1454	$22000 \pm^{2260}_{250}$	8.00	L1	DA:ire		JHK	PB4150	SD
1416+1352	$38000 \pm^{20800}_{6750}$	8.00	M6	DA:ire		JHK	PK_003+66_1	Galaxy
1423-0138	$16000 \pm^{380}_{60}$	$8.00 \pm^{0.21}_{0.41}$	$\geq L8$:	DA:ire:	moreIR	JH		
1441+0137	$26000 \pm^{60}_{420}$	8.00	L6:	DA:ire:	bf:	JHK	PG1438+018	SD

Table 8 – *continued*

Coord	T _{eff} (K)	log(<i>g</i>)	Companion	Notes	Notes2	JHK	Simbad Name	Simbad Class
1442+0910	20000± ¹⁷⁰ ₁₄₀	7.75± ^{1.13} _{0.59}	M7	DA:ire		JHK		
1448+0812	24000± ¹¹⁵⁰ ₃₃₈₀	8.00	M7	DA:ire		JHK	WD1446+028	DA
1455+0458	30000± ²³⁸⁰ ₂₄₀	8.00	M8	DA:ire		JHK		
1456+1040	14000± ¹⁴³⁰ ₁₅₈₀	8.75± ^{0.91} _{0.75}	L1:	DA:ire		JHK		
1507+0724	26000± ²⁴⁰⁰ ₂₃₄₀	8.00	M7	DA:ire		JHK		
1523+0023	24000± ¹³⁶⁰ ₂₃₃₀	8.00	M8	DA:ire		JHK		
1524−0128	18000± ²⁰ ₂₀	9.25± ^{0.02} _{0.16}	≥L8:	DA:ire:	bf	JHK	BPS_CS_22890−0079	SD
1527+0802	20000± ¹⁵³⁰ ₈₃₀	9.50± ^{0.63} _{0.28}	≥L8:	DA:ire:		JHK		
1538+0644	10000± ⁵⁰ ₄₀	7.25± ^{0.10} _{0.02}	L6	DA:ire:	bf:	JHK		
1538+2957	20000± ⁴⁰ ₁₂₀	5.75± ^{0.75} _{0.84}	M7:	DA:ire		JHK		
1540+2908	34000± ⁴²⁷⁰ ₁₂₄₀	8.00	M7	DA:ire		JH		
1548+0006	14000± ⁵⁰ ₅₀	8.50± ^{0.08} _{0.04}	L6:	DA:ire:		JHK		
1549+0325	13000± ³⁰⁰ ₁₇₀	7.25± ^{0.64} _{0.52}	L7:	DA:ire:	bf	JHK	PG1546+036	UV
1551−0118	13000± ⁷⁰ ₁₀₄₀	8.25± ^{0.29} _{0.28}	≥L8:	DA:ire:	bf	JHK		
1554+0616	17000± ⁶³⁰ ₂₀₀	7.25± ^{1.57} _{0.88}	M6	DA:ire:	resolved,bg:	JHK		
1614+2235	20000± ¹⁰⁰ ₁₀₉₀	8.50± ^{0.56} _{0.74}	L6	DA:ire		JHK	SDSS	SD
1635+2912	17000± ¹⁰⁰ ₁₀₃₀	5.50± ^{0.50} _{0.93}	L6:	DA:ire:	moreIR,disk:,bg:	JHK		
2042+0055	28000± ²¹⁶⁰ ₃₅₀	8.00	≥L8:	DA:ire:	bf:	HK		
2049−0001	16000± ¹¹⁶⁰ ₃₈₀	8.75± ^{0.82} _{0.45}	≥L8:	DA:ire:	bf:	HK		
2052+0018	12000± ¹⁰⁸⁰ ₁₃₀	8.00± ^{0.34} _{0.24}	≥L8:	DA:ire:	bf:	HK		
2117−0015	12000± ¹²⁰ ₁₄₀	8.00± ^{0.15} _{0.05}	≥L8:	DA:ire:	bf:	HK		
2135−0031	30000± ¹³⁹⁰ ₂₅₉₀	8.00	M7	DA:ire		JHK		
2147−0112	26000± ²¹⁹⁰ ₃₉₀	8.00	L1:	DA:ire	resolved:	JHK	2MASS	Blue
2308+0658	28000± ¹²⁶⁰ ₂₁₄₀	8.00	M6	DA:ire		JHK		
2326+1230	18000± ²⁰⁰ ₁₈₀	8.75± ^{0.58} _{0.29}	≥L8:	DA:ire:	bf:	JHK	2MASS	Star
2330+1450	13000± ¹⁵⁸⁰ ₄₀₀	9.50± ^{0.64} _{0.24}	≥L8:	DA:ire:	bf:	JHK		
2335+1047	11000± ⁵²⁰ ₄₅₀	7.75± ^{0.55} _{0.46}	L4	DA:ire:	resolved,bg:	JHK		
2344+0817	8000± ¹⁰⁰ ₄₁₀	8.00	L8:	DA:ire:	bf:	JHK	PB5517	Star
2348+0200	8000± ³⁰ ₁₀	8.00	L6:	DA:ire:	QSO:	JHK		

Table 9. IR excess candidates which are found to have an excess in either the spectroscopic or photometric-only methods, but all have an SDSS spectrum for classification. The table follows the same format as Table 7 and 8, with addition that S and P in the titles refers to the spectroscopic and photometric methods respectively. Fiber and fit parameters are only shown if an IR excess was found in the corresponding method.

Coord	S $T_{\text{eff}} (K)$	S $\log(g)$	P $T_{\text{eff}} (K)$	P $\log(g)$	S Companion	P Companion	Notes	S Notes	P Notes	Classification	Simbad Name	Simbad Class
0018+0101			22000 \pm ²²⁰ ₅₀	8.00 \pm		L1	DA:ire			NLHS		
0032+0739	21045 \pm 249	7.42 \pm 0.05			M6		DAire:	resolved,bg:		DA		
0039–0030	12392 \pm 544	7.35 \pm 0.16	11000 \pm ⁵⁰ ₂₀	7.75 \pm ^{0.10} _{0.03}	M9	L2	DAire:			DA		
0118–0025			26000 \pm ⁸⁸⁰ ₇₈₀	8.00 \pm		L3	DA:ire		resolved	NLHS		
0135+1445	7467 \pm 18	7.34 \pm 0.04	8000 \pm ¹⁰ ₂₀	8.00 \pm	L6	L8	DAire			DA		
0207+0702	10073 \pm 77	8.32 \pm 0.09	15000 \pm ¹⁰⁹⁰ ₃₆₀	8.75 \pm ^{0.89} _{0.28}	L7	?	DAire:		bf	DA		
0236–0103	20566 \pm 498	7.66 \pm 0.09	18000 \pm ¹³⁹⁰ ₁₂₀₀	8.75 \pm ^{2.48} _{0.75}	M6	\geq L8:	DAire		bf	DA		
0253–0027	18974 \pm 286	7.71 \pm 0.06			L4		DAire	moreIR		DA		
0333+0020			22000 \pm ²³⁶⁰ ₃₉₀	8.00 \pm		M9	DA:ire			NLHS		
0748+2058	86726 \pm 7732	7.15 \pm 0.27	40000 \pm ³⁶⁴⁰ ₃₆₂₀	8.00 \pm	M3	M5	DAire	resolved:	resolved:	DA		
0753+2447	13432 \pm 710	7.81 \pm 0.15	12000 \pm ¹¹³⁰ ₂₉₀	7.75 \pm ^{0.45} _{0.41}	L5:	L6:	DAire	disk		DA		
0814+2811			9000 \pm ⁵⁹⁰ ₄₀	8.50 \pm ^{0.43} _{0.53}		\geq L8:	DA:ire:		bf	NLHS		
0847+2831	12828 \pm 930	7.76 \pm 0.20	12000 \pm ²⁰⁹⁰ ₁₀₃₀	8.25 \pm ^{1.22} _{1.04}	M6	M9	DAire			DA		
0851+0330			20000 \pm ²⁰⁹⁰ ₂₇₄₀	9.50 \pm ^{1.55}		L6	DA:ire			WDMS		
0907+0536	19416 \pm 458	7.78 \pm 0.09			L6		DAire:	moreIR		DA		
0933+3200	11565 \pm 381	8.36 \pm 0.20	10000 \pm ¹⁰⁷⁰ ₇₀	7.50 \pm ^{0.36} _{0.23}	L4	L2	DAire	resolved:	resolved:	DA		
0950+0115	21785 \pm 365	7.89 \pm 0.06			L8		DAire:	moreIR		DA		
0951+0347			24000 \pm ¹⁰⁰ ₂₀₄₀	8.00 \pm		\geq L8:	DA:ire:		bf	NLHS		
1002+0939	21785 \pm 808	7.92 \pm 0.14	20000 \pm ¹⁴⁰ ₁₀₀	8.00 \pm ^{0.48} _{0.52}	L0	L0	DAire			DA		
1010+0407	13588 \pm 668	7.76 \pm 0.11			L8:		DAire:	moreIR		DA		
1015+0425	34526 \pm 86	7.38 \pm 0.07			L4		DAire:	moreIR		DA		
1016+0020	21045 \pm 703	8.48 \pm 0.12			L6		DAire:	moreIR		DA		
1025+1200			22000 \pm ⁶¹⁰ ₃₇₀	8.00 \pm		L1	DA:ire			NLHS		
1037+0139	11433 \pm 208	8.38 \pm 0.13	15000 \pm ³⁶⁰ ₁₂₇₀	8.50 \pm ^{0.34} _{0.66}	L5:	L1	DAire			DA		
1100+0346			32000 \pm ⁶⁹²⁰ ₃₁₃₀	8.00 \pm		M7	DA:ire			NLHS		
1106+0737			28000 \pm ³⁸⁰⁰ ₂₀₆₀	8.00 \pm		M5	DA:ire			WDMS		
1120+0639	20331 \pm 609	7.69 \pm 0.11			L3		DAire:	resolved,bg:		DA		
1135+0731			8000 \pm ⁸⁰ ₇₀	8.00 \pm		L7:	DA:ire:		bf:	NLHS		
1141+0420	11835 \pm 818	7.37 \pm 0.22	12000 \pm ²³⁰ ₁₀₈₀	7.50 \pm ^{0.48} _{0.35}	M7	M7	DAire			DA		
1148+0336			28000 \pm ²⁵⁰ ₂₀₀₀	8.00 \pm		L0	DA:ire			NLHS		
1148+0640			24000 \pm ³⁷¹⁰ ₁₃₈₀	8.00 \pm		M8	DA:ire			NLHS		
1208+0610	23076 \pm 1125	7.64 \pm 0.17	20000 \pm ⁴²⁰ ₁₁₂₀	8.75 \pm ^{1.03} _{0.75}	M7	L3	DAire			DA		
1211+1437			24000 \pm ⁷⁴⁰ ₂₄₇₀	8.00 \pm		M9	DA:ire			NLHS		
1212+0136			10000 \pm ⁸⁰ ₇₀	7.75 \pm ^{0.25} _{0.06}		?	DA:ire:		bf	MWD		
1215+1351			24000 \pm ³⁵⁰ ₂₁₈₀	8.00 \pm		M6	DA:ire:		resolved:	NLHS		
1218+0042	11173 \pm 180	8.30 \pm 0.11	10000 \pm ¹³⁰ ₃₀	7.75 \pm ^{0.07} _{0.08}	L8	L8:	DAire:	moreIR	moreIR	DA		
1219+1244			10000 \pm ³³⁰ ₅₃₀	7.50 \pm ^{0.50} _{0.34}		L8:	DA:ire:	No–Xs	bf:	DA		
1228+1040	22037 \pm 199	8.19 \pm 0.04	20000 \pm ¹⁰ ₁₀	8.50 \pm ^{0.03} _{0.13}	L6:	L8:	DAire	disk	disk	DA		
1246+0707	10793 \pm 189	8.03 \pm 0.16	9000 \pm ¹⁰¹⁰ ₅₀	7.00 \pm ^{0.15} _{0.35}	L2	M8	DAire			DA		
1247+1035	17912 \pm 159	7.82 \pm 0.04			L6:		DAire:	bg;:,resolved:		DA		
1249+0422			11000 \pm ¹⁰ ₁₀	8.00 \pm ^{0.03} _{0.01}		L8:	DA:ire:	No–Xs	moreIR	DA		
1250+1549			9000 \pm ¹⁰⁶⁰ ₉₀	8.50 \pm ^{0.62} _{0.72}		L3:	DA:ire:		bf	MWD		
1300+0057			26000 \pm ²⁰⁰⁰ ₆₈₀	8.00 \pm		\geq L8:	DA:ire:		bf:	NLHS		
1310+0233			26000 \pm ²⁴⁰ ₃₄₀	8.00 \pm		M8	DA:ire			NLHS		

Table 9 – *continued*

Coord	S $T_{\text{eff}} (K)$	S $\log(g)$	P $T_{\text{eff}} (K)$	P $\log(g)$	S Companion	P	Notes	S Notes	P Notes	Classification	Simbad Name	Simbad Class
1314+0057	17707 \pm 163	7.80 \pm 0.04	17000 \pm^{1050}_{510}	8.25 $\pm^{1.21}_{0.60}$	L6	\geq L8:	DA:ire:	disk:	bf	DA		
1320+0018	19193 \pm 213	8.40 \pm 0.04	19000 \pm^{580}_{370}	8.75 $\pm^{0.61}_{0.64}$	L8	L8:	DA:ire:	disk:	disk:	DA		
1329+1230	13432 \pm 272	7.42 \pm 0.05	12000 \pm^{80}_{80}	7.50 $\pm^{0.26}_{0.09}$	M7	M8	DA:ire:			DA		
1331+0040	15964 \pm 714	7.72 \pm 0.17			?		DA:ire:	moreIR		DA		
1334+0647			8000 \pm^{20}_{20}	8.00 \pm		\geq L8:	DA:ire:	No–Xs	moreIR	DA		
1341+0056	18330 \pm 436	7.99 \pm 0.10	17000 \pm^{530}_{1050}	7.75 $\pm^{1.16}_{0.94}$	M7	M6:	DA:ire:			DA		
1352+0910	36154 \pm 722	7.49 \pm 0.11	28000 \pm^{1080}_{2300}	8.00 \pm	M5	M6	DA:ire:			DA		
1410+0225	11565 \pm 246	8.63 \pm 0.13	11000 \pm^{0}_{0}	8.00 $\pm^{0.01}$	\geq L8	L8	DA:ire:	moreIR	moreIR	DA		
1414+0212			8000 \pm^{20}_{20}	8.00 \pm		\geq L8:	DA:ire:	No–Xs	moreIR, bf:	DA		
1415+0117			32000 \pm^{4360}_{2230}	8.00 \pm		M6	DA:ire:			WDMS		
1422+0920			22000 \pm^{520}_{630}	8.00 \pm		M9:	DA:ire:			NLHS		
1424+0319			30000 \pm^{50}_{20}	8.00 \pm		L5	DA:ire:		hotWD	NLHS		
1425–0013	10670 \pm 169	7.97 \pm 0.17			L8:		DA:ire:	moreIR		DA		
1436+0138			24000 \pm^{590}_{90}	8.00 \pm		L4	DA:ire:		moreIR	NLHS		
1443+0931			26000 \pm^{1600}_{890}	8.00 \pm		M9	DA:ire:			NLHS		
1448+0240	14728 \pm 247	7.41 \pm 0.06	13000 \pm^{1030}_{130}	8.00 $\pm^{0.52}_{0.19}$	L4	L6	DA:ire:	moreIR	moreIR	DA		
1448+0713	12250 \pm 256	7.87 \pm 0.09	11000 \pm^{1130}_{440}	7.75 $\pm^{0.55}_{0.62}$	M8	M9	DA:ire:			DA		
1450+0000	17106 \pm 175	7.93 \pm 0.05			L8:		DA:ire:	moreIR		DA		
1500+0642			26000 \pm^{110}_{2000}	8.00 \pm		L1:	DA:ire:			NLHS		
1510+0409			28000 \pm^{560}_{2000}	8.00 \pm		M8	DA:ire:			NLHS		
1514+0744			10000 \pm^{60}_{230}	8.50 $\pm^{0.30}_{0.42}$		L5:	DA:ire:		bf	MWD		
1519+0715			26000 \pm^{80}_{80}	8.00 \pm		M7	DA:ire:		moreIR	NLHS		
1525+0958			28000 \pm^{2120}_{280}	8.00 \pm		M9	DA:ire:			NLHS		
1539+2706			28000 \pm^{330}_{670}	8.00 \pm		M9	DA:ire:	bf		DA		
1541+0417			24000 \pm^{230}_{240}	8.00 \pm		L2	DA:ire:			NLHS		
1543+0012			17000 \pm^{2110}_{2920}	9.50 $\pm^{0.81}$		L8:	DA:ire:		bf	NLHS		
1557+0916	22811 \pm 734	7.75 \pm 0.11	18000 \pm^{1050}_{130}	7.75 $\pm^{0.83}_{0.41}$	L1:	L5	DA:ire:			DA		
1609+2905	8773 \pm 91	8.26 \pm 0.14	9000 \pm^{70}_{140}	7.75 $\pm^{0.41}_{0.31}$	\geq L8	L8	DA:ire:			DA		
1614+2616			24000 \pm^{150}_{220}	8.00 \pm		L5	DA:ire:			NLHS		
1619+2407			9000 \pm^{180}_{210}	8.75 $\pm^{1.02}_{0.75}$		\geq L8:	DA:ire:		bf	NLHS		
1619+2533	25595 \pm 1139	7.21 \pm 0.15	18000 \pm^{2080}_{1390}	9.50 $\pm^{1.89}$	M5	L6:	DA:ire:		bf	DA		
1625+3026	72136 \pm 4550	7.77 \pm 0.19	40000 \pm^{11380}_{4690}	8.00 \pm	M5	M6	DA:ire:			DA		
1637+3113			26000 \pm^{400}_{270}	8.00 \pm		M9	DA:ire:			NLHS		
1640+3117			26000 \pm^{3230}_{2780}	8.00 \pm		M7	DA:ire:			NLHS		
1645+3109			17000 \pm^{2510}_{1970}	9.50 $\pm^{1.24}$		\geq L8:	DA:ire:		bf:	NLHS		
2038+0109			20000 \pm^{2100}_{620}	9.00 $\pm^{1.23}_{0.50}$		\geq L8:	DA:ire:		bf:	NLHS		
2117–0006			8000 \pm^{20}_{10}	8.00 \pm		\geq L8:	DA:ire:		bf:	NLHS		
2118+0028			15000 \pm^{230}_{40}	8.25 $\pm^{0.17}_{0.21}$		\geq L8:	DA:ire:	No–Xs	bf:,resolved,bg:	DA		
2220–0041	7467 \pm 21	7.66 \pm 0.12	8000 \pm^{20}_{30}	8.00 \pm	\geq L8	\geq L8:	DA:ire:	resolved	resolved,bg:	DA		
2225+0016	11045 \pm 235	8.44 \pm 0.16	9000 \pm^{20}_{20}	7.00 $\pm^{0.26}_{0.08}$	L6	L5	DA:ire:	resolved:	resolved:,bg:	DA		
2255–0015			17000 \pm^{170}_{620}	9.00 $\pm^{0.25}_{0.37}$		L4:	DA:ire:		bf:,resolved,bg:	WDMS		
2331+1342	11173 \pm 284	8.79 \pm 0.15	15000 \pm^{1230}_{1600}	9.50 $\pm^{0.73}$	L6	L8	DA:ire:			DA		

Table 10. The 19 IR excess candidates from both the spectroscopic and photometric fitting methods that are also found to be white dwarf + main sequence binaries in Rebassa-Mansergas et al. (2010). Objects from the spectroscopic and photometric IR excess candidates are denoted as "S" and "P" in the "Method" column respectively. The first set of system parameters are from the methods described herein. Where both spectroscopic and photometric IR excesses were found, the quoted parameters are those from the spectroscopic method, the second from Rebassa-Mansergas et al.. In some cases, such as SDSS J0207+0702, the two spectroscopic fitting techniques disagree significantly, this is where a different hot/cold fit solution was chosen. Photometric temperatures may also disagree significantly from the Rebassa-Mansergas et al. (2010) temperatures as discussed in Section 5.1.2. The columns labelled with a "R-M" prefix are the best fit taken from Table 7 of Rebassa-Mansergas et al. (2010). R-M Sp=-1 indicates that no spectral type could be associated.

Name	T _{eff}	log(<i>g</i>)	Method	Companion	Notes	R-M T _{eff}	R-M log(<i>g</i>)	R-M Sp
0032+0739	21045 ± 249	7.42 ± 0.05	S	M6	DAire:	21045 ± 371	7.43 ± 0.07	M2
0039-0030	12392 ± 544	7.35 ± 0.16	SP	M9	DAire:	12392 ± 737	7.39 ± 0.22	-1
0207+0702	10073 ± 77	8.32 ± 0.09	SP	L7	DAire:	18756 ± 502	7.42 ± 0.10	-1
0236-0103	20566 ± 498	7.66 ± 0.09	SP	M6	DAire	21289 ± 723	7.83 ± 0.13	M8
0748+2058	86726 ± 7732	7.15 ± 0.27	SP	M3	DAire	87731 ± 10728	7.17 ± 0.38	M2
0847+2831	12828 ± 930	7.76 ± 0.20	SP	M6	DAire	13588 ± 923	7.76 ± 0.18	M6
0851+0330	20000 ⁺²⁷⁴⁰ ₋₂₀₉₀	9.50 ^{+0.00} _{-1.55}	P	L6	DA:ire	22550 ± 520	7.40 ± 0.08	M6
1037+0139	11433 ± 208	8.38 ± 0.13	SP	L5:	DAire	16717 ± 602	7.78 ± 0.14	M5
1106+0737	28000 ⁺²⁰⁶⁰ ₋₃₈₀₀	8.00	P	M5	DA:ire	36154 ± 540	7.74 ± 0.09	M5
1141+0420	11835 ± 818	7.37 ± 0.22	SP	M7	DAire	12110 ± 780	7.39 ± 0.26	-1
1329+1230	13432 ± 272	7.42 ± 0.05	SP	M7	DAire	12250 ± 1036	7.47 ± 0.20	-1
1341+0056	18330 ± 436	7.99 ± 0.10	SP	M7	DAire	18330 ± 608	8.01 ± 0.13	-1
1352+0910	36154 ± 722	7.49 ± 0.11	SP	M5	DAire	35331 ± 919	7.31 ± 0.16	-1
1415+0117	32000 ⁺²²³⁰ ₋₄₃₆₀	8.00	P	M6	DA:ire	73816 ± 4981	8.43 ± 0.18	M0
1448+0713	12250 ± 256	7.87 ± 0.09	SP	M8	DAire	12110 ± 264	7.84 ± 0.13	M6
1539+2706	28000 ⁺⁶⁷⁰ ₋₃₃₀	8.00	P	M9	DA:ire	36572 ± 447	7.31 ± 0.07	-1
1619+2533	25595 ± 1139	7.21 ± 0.15	SP	M5	DAire	25891 ± 1447	7.30 ± 0.20	-1
2255-0015	17000 ⁺⁶²⁰ ₋₁₇₀	9.00 ^{+0.37} _{-0.25}	P	L4:	DA:ire:	22550 ± 724	7.88 ± 0.12	M6
2331+1342	11173 ± 284	8.79 ± 0.15	SP	L6	DAire	18756 ± 1020	7.96 ± 0.20	-1